UNITED NATIONS UNIVERSITY
UNU-GTP
Geothermal Training Programme

Orkustofnun, Grensasvegur 9,
IS-108 Reykjavik, Iceland

Reports 2016
Number 34

A 3D MODEL OF THE CHACHIMBIRO GEOTHERMAL SYSTEM IN ECUADOR USING PETREL

Byron F. Pilicita Masabanda
Corporación Eléctrica del Ecuador
Unidad de Negocio Termopichincha
Av. 6 de Diciembre N26-235 y Av. Orellana, Quito
ECUADOR
bf07epn@gmail.com

ABSTRACT

The Chachimbiro Geothermal System is the most important geothermal prospect in Ecuador. Various geothermal models have been presented based on geological, geochemical and geophysical data collected at different epochs. Currently the Chachimbiro prospect is ready to enter the exploration drilling phase. This is why it is important to identify the best drilling targets. The Petrel software allows the combination of all surface exploration data in order to identify different geothermal anomalies and create a 3D model to visualize all features of the system. This model uses lineaments as boundaries of the system based on structural mapping and locations of earthquake epicentres. The heat source is related to magma chambers that feed the main volcanic vent but is also controlled by faults, which influence possible up-flow. This up-flow is located beneath a cap rock (0-10 Ωm) and is related to a high resistivity core, which shows a concave shape (30-70 Ωm). The Na/K geothermometers show temperatures of around 240°C, however, the water in Chachimbiro has poor equilibrium with the rock. Resistivity analysis shows possible temperatures from 200 to 250°C, but this range of temperature does not represent the current temperature of the system. The origin of the fluids in Chachimbiro is meteoric based upon isotopic analysis. The interaction between this fluid, with the up-flow into the sub-surface, forms a possible reservoir. Hot springs and gas manifestations (CO_2-H_2S) are out-flows of the system, which also indicate volcanic activity in the system and are expressions of the reservoir at the surface. The intersection between Chachimbiro and Azufral faults and the Chachimbiro Fault have been identified as drilling targets in the system, which could be reached by directional drilling from three different locations. These location have been chosen by combining the structural features, the resistivity anomalies, possible out-flow and up-flow zones, the hydrothermal areas and temperature anomalies which were modelled and analysed in Petrel.

1. INTRODUCTION

Conceptual models are based on geological information, both from surface mapping and analysis of subsurface data, remote sensing data, results of geophysical surveying, information on chemical and isotopic content of fluid at surface manifestations and reservoir fluid samples collected from wells,

information on temperature and pressure conditions based on analysis of available well logging data as well as other reservoir engineering information. These data are processed in order to explain the heat source that feed the reservoir, to locate the recharge zones and the main flow channels, and to analyse the general flow patterns within the reservoir as well as reservoir temperature and pressure conditions. A comprehensive conceptual model furthermore, provides an estimate of the size of the reservoir. Nevertheless, not all geothermal conceptual models incorporate the whole information at the same time, in fact only a few do so. In the early stages, the conceptual models depend mostly on surface exploration data, with geological (e.g. faults/fractures) and geophysical (e.g. resistivity) data being most important. Formation temperature is e.g. unknown at such an early stage. The only indications of reservoir temperature at that stage come from chemical investigation (Axelsson, 2013).

Three-dimensional modelling software is increasingly being used to visualize, merge and jointly analyse various types of data in geothermal research. The Petrel E&P is software that provides a full range of tools to solve the most complex challenges from regional exploration to reservoir development. Petrel allows the integration of structural geology, lithology, geochemical and geophysical data obtained in the early stages of the geothermal system development (Schlumberger, 2016). Chachimbiro is a geothermal prospect is currently at the pre-feasibility stage. The area is located on the eastern slopes of the Western Cordillera, at about 70 km north of Quito, which is Ecuador's capital and 18 km west of Ibarra which is the nearest major load centre. It is bounded to the north by Chota Basin, to the east by Interandean valley, to the south and west by Cotocachi and Yanahurcu de Piñan volcanoes, respectively (Figure 1).

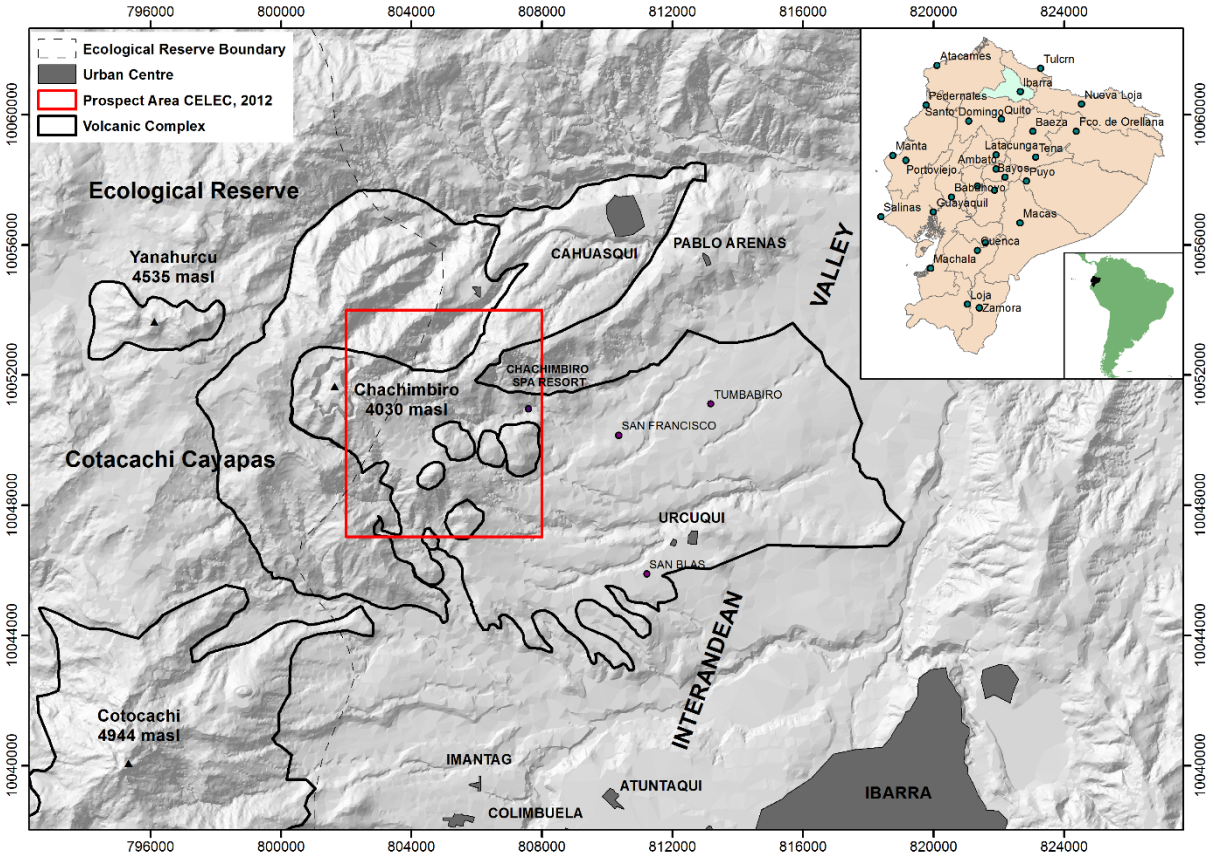

FIGURE 1: Location of the Chachimbiro volcanic complex

The area straddles the Cotacachi – Cayapas Ecological Reserve. It is only accessible by gravel and dirt roads. The climate is temperate and the vegetation cover varies from forest to grassy areas. In administrative terms, the area is divided into 3 parishes: Urcuquí, San Blas and Tumbabiro and it belongs to the Urcuquí district in the Imbabura province. The best-known hot springs in the area are located along the Cachiyacu River, in the Spa Resort Chachimbiro area. La Delicia de San Francisco is the nearest habitation to the hot springs.

Previous work has been carried out at Chachimbiro with the objective to assess the geothermal potential of the area. These studies where completed by government institutions between the late 70s and early 90s, within the framework of OLADE-INECEL[1], OLADE-AQUATER[2] and IAEA[3]-INECEL projects. In 2011, CELEC EP[4] (Government Company) contracted the SYR[5] Company to gather geoscience information and develop a Geothermal Conceptual Model, which was presented in 2012 (SYR, 2012). Currently CELEC EP is being assisted by JICA (Japan International Cooperation Agency) to gather complementary information about Chachimbiro Geothermal System together with MMC-MMTEC[6] Consultants Company.

This report summarizes the geothermal model of the Chachimbiro Geothermal System in the Petrel E&P software platform. By integrating the results of geological, geochemical and geophysical studies obtained by CELEC EP / SYR in 2012 and results from CELEC EP / MMC in 2016, the objective is to visualize the features of the conceptual models, to propose new study areas and to recommend locations and targets of wells which may be drilled in the future.

2. GEOLOGICAL AND GEODYNAMIC SETTING

Regional features are identified as fragmentations of the Farallón Plate, forming the Cocos and Nazca Plate during the early Miocene (Lonsdale, 2005). The interaction between the South American, Cocos and Nazca plates control the cortical deformation, the high seismicity and the volcanism in the North-Andean Block (Figure 2). The convergence between the Nazca and South American plates is estimated to be 7.0 cm/year (Schellart et al., 2007). The tectonic state of stress is homogenous south of 5°N; this state results in an East-West-oriented compression which is responsible for the crustal deformation (Ego et al., 1996).

The Chachimbiro Volcanic Complex consists of 60 volcanoes associated with the Ecuadorian Quaternary Volcanic Arc. It is located 80 km north of Quito, in the northern part of the Ecuadorian Volcanic Front. Holocene activity is characterized by powerful, but low-frequency, explosive eruptions of acid andesite to dacite magmas. The long-lasting evolution of the Chachimbiro Volcanic Complex comprises three successive phases named Huanguillaro, Tumbatú, and Hugá. Recent investigations identified at least four eruptions associated to the Hugá phase in the last 6,000 years (Bernard et al., 2014).

The basement of the Chachimbiro Volcanic Complex is composed of Cretaceous rocks that accreted in a subduction zone. McCourt et al. (1997) and Vallejo (2007) defined the Pallatanga Formation as the volcanic basement of the Western Cordillera, which comprises mainly basaltic rocks. There are no outcrops in the Chachimbiro volcanic area, but it probably lies under the distal southeast flanks of the volcano. Vallejo (2007) described the Rio Cala Group, which is composed of volcanic and sedimentary sequence deposited in an intraoceanic island arc setting, overlying the Pallatanga formation. It consists of massive basaltic to andesitic lavas, volcanic breccias, and to a smaller extent, of volcanoclastic sandstones. This unit is exposed on the Southeastern flank of the volcanic complex. The Natividad formation included in the Rio Cala Group, is composed of sedimentary rocks in the north of the volcanic complex, correlated with turbidites deposited during the Eocene (Vallejo 2007). The Natividad Unit is exposed on both the southwestern and northeastern slopes of the volcano and is probably the dominant Cretaceous lithology underlying the southern and eastern slopes of the Chachimbiro Volcanic Complex (Granda, 2011). The Silante formation is restricted to the northern area of the Western Cordillera, which

[1] Latin American Energy Organization (OLADE), the Ecuadorian Institute of Electrification (INECEL)
[2] Decision Support System to manage water resources in Italy using remote sensing (AQUATER)
[3] International Atomic Energy Agency (IAEA)
[4] Corporación Eléctrica del Ecuador (CELEC EP)
[5] Servicios y Remediación (SYR)
[6] Mitsubishi Materials Corporation - Mitsubishi Materials Techno Corporation (MMC-MMTEC)

includes channelized conglomerates, breccias, red mudstones and shales, deposited during the latest Maastrichtian to Early Paleocene (Vallejo 2007). The unit is clearly exposed on the western and northern flanks of the volcanic complex and, most likely, underlies the western half of the volcano (Granda, 2011).

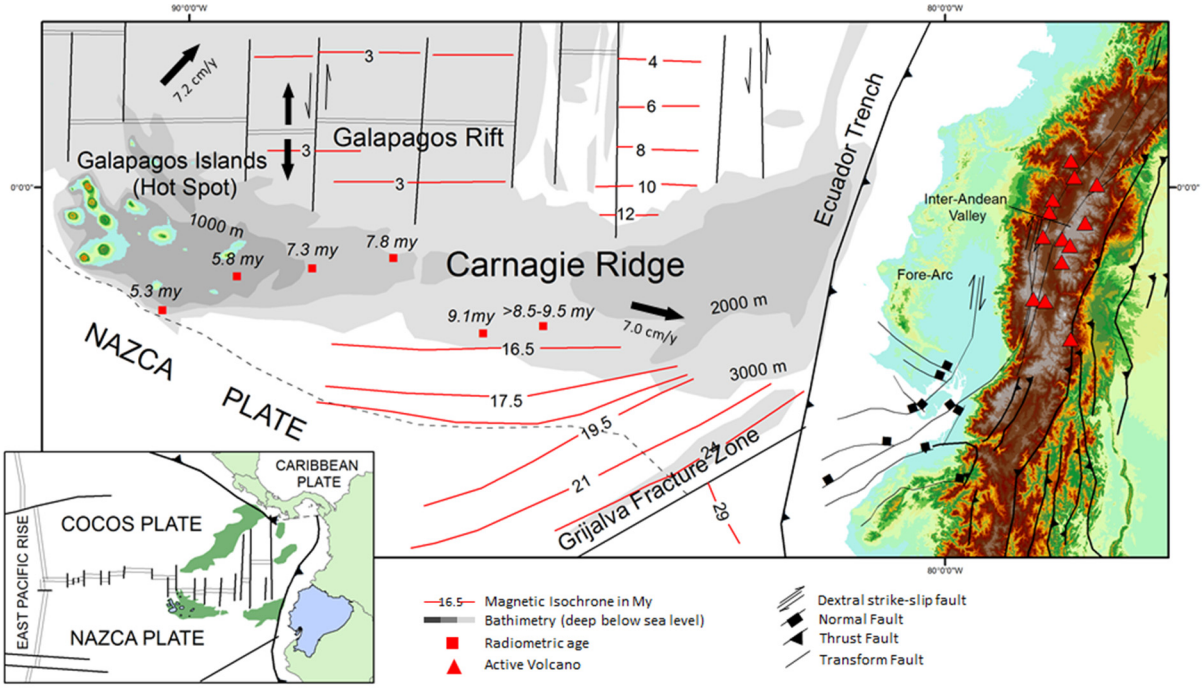

FIGURE 2: Geodynamic setting of Ecuador, showing mainland Ecuador on the South American plate and the Galapagos Islands on the Nazca plate (redrawn after the plate tectonic map of the Circum-Pacific Region (1981) and modified from Spikings et al., 2001)

The Pugaran volcanic rocks were deposited during the Tertiary, and occur both southeast and northwest of the Chachimbiro volcanic complex. This volcanic unit consists of andesitic lava flows and hornblende dacite tuffs and breccias. There is no evidence whether the Pugaran unit extends beneath the Chachimbiro volcanic complex (Granda, 2011).

Chachimbiro Phase 1 is composed of large andesite lava flows streaming radially and predominantly effusive events. These lavas form the ancestral andesitic stratovolcano known as Huanguillaro (Beate, 1990 in SYR 2012). After phase 1, an instability in the volcanic complex centre resulted in a collapse forming a horseshoe shaped scarp, which is open to the east (Figure 3 and 4).

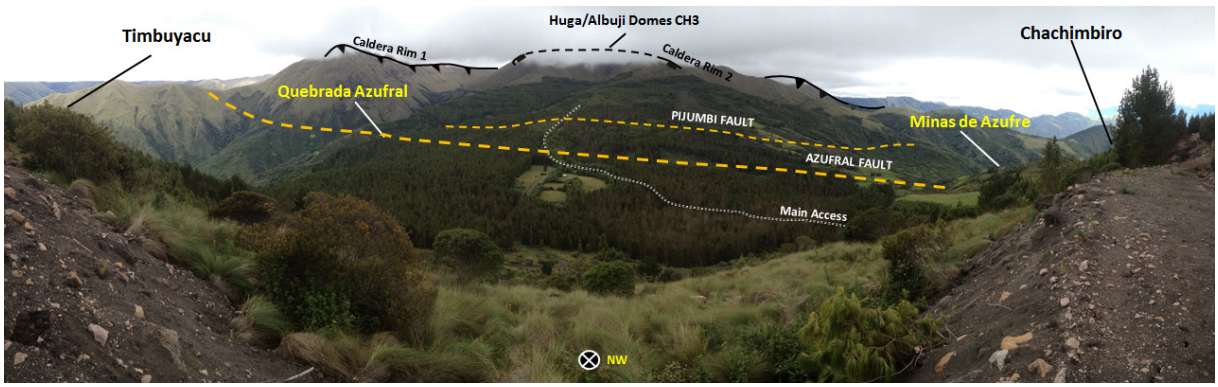

FIGURE 3: Panoramic view of Chachimbiro volcanic complex with the main geothermal manifestation areas and fault structures

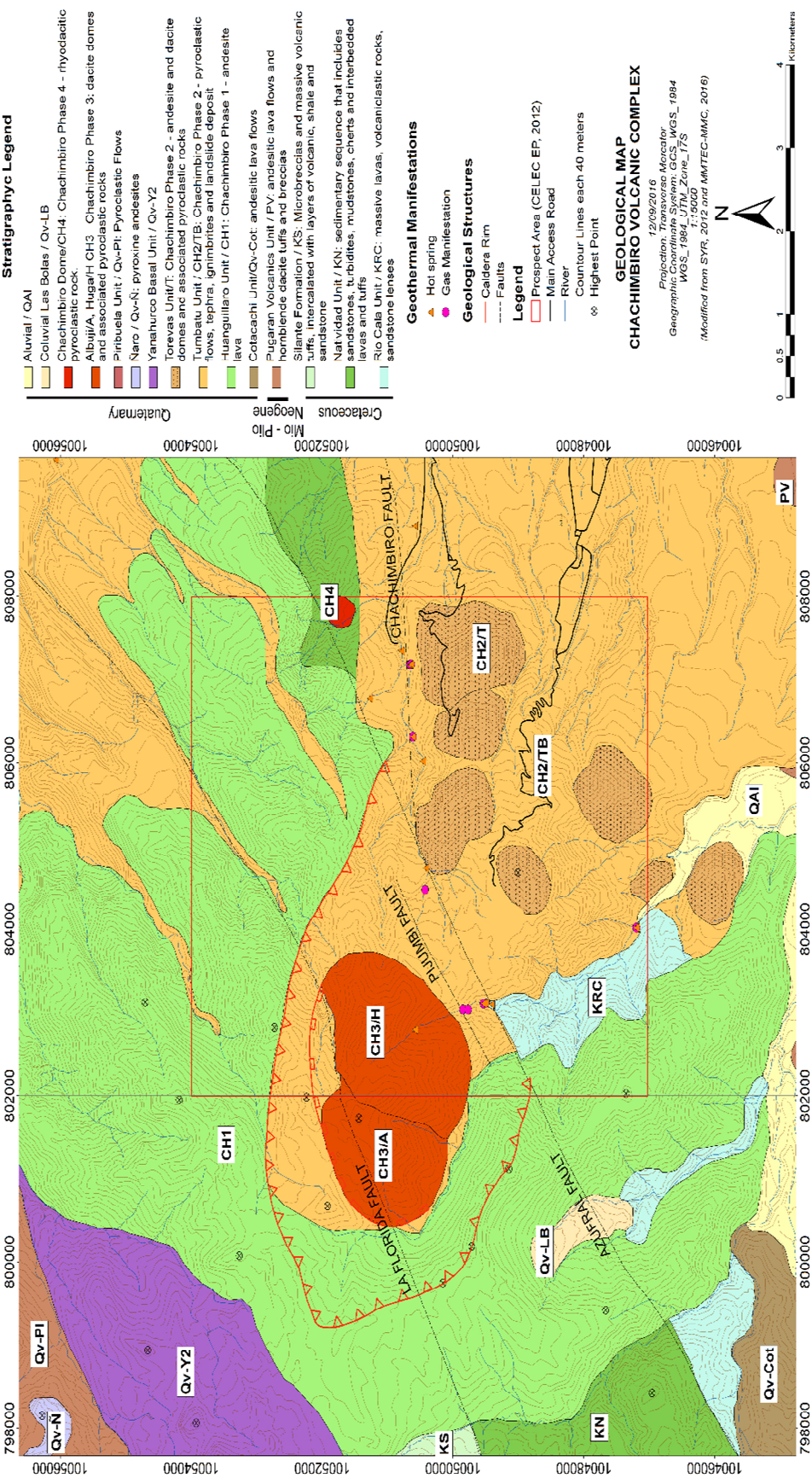

FIGURE 4: Geological Map of Chachimbiro volcanic complex, Ecuador, 1:15000 (modified from SYR, 2012)

The Quaternary volcanics evolved in four distinct phases (Bernard et al., 2010; 2014), which form the Chachimbiro Volcanic Complex and lie unconformable on the Cretaceous rocks.

Chachimbiro Phase 2 is described as either the Tumbatú or Chachimbiro volcano. Following this phase of dacitic dome building a second landslide occurred, with land mass movement to the east and the development of a smaller scarp that is sub-parallel to the scarp associated with the first collapse (Figure 3). Ruiz G. (2011), following Bernard et al. (2010), mapped these dacite domes as torevas, indicating that they may have been displaced from their point of origin while preserving some of their original morphology (Figure 4)

Chachimbiro Phase 3 in the evolution of the Chachimbiro Volcanic Complex is the most recent period of dome building, extending into the Holocene (Bernard et al., 2010). These large and young dacitic domes occupy the centre of the crater that resulted from the second landslide and include the large domes of Cerro Hugá and Cerro Albují (Figures 3 and 4). These domes and associated pyroclastics are predominantly dacitic, although some andesites are also observed (SYR, 2012).

Chachimbiro Phase 4 which was recently described by Bernard et al. (2014), occurred on the northeast slope of the volcano and defined the most powerful Holocene eruption of the Chachimbiro volcano, dated between 3640 and 3510 years BC. It produced a large pyroclastic density current directed to the southeast followed by a sub-Plinian eruptive column drifted westwards by the wind.

In the final report by SYR (2012), three fault systems were identified, believed to play important roles in the origin of the volcano and the potential location and circulation in the geothermal system.

The NE-SW striking Florida fault system forms the contact between the Cretaceous Natividad and Silante units. This fault complex underlies the eruptive centres of the Huanguarillo volcano and the Hugá-Albuji domes (Figure 4).

The Azufral fault system in the central part of the project area also trends NE-SW. Based on structural mapping information collected by SYR it is interpreted as being a right lateral strike slip fault system. This fault zone, which may represent the transition of the Natividad to the Rio Cala formations, brings the Rio Cala unit into contact with the Quaternary volcanic unit. The fault system is described as two separate segments – the Pijumbí fault and the Crusacha fault (SYR, 2012), but according to a new report by MMC-MMTEC (2016) the Pijumbi fault is a segment parallel to the Azufral Fault (Figures 3 and 5). The third important fault zone is an unnamed fault system that extends EW through the eastern part of the Chachimbiro. Nevertheless, in the new geological report by MMC-MMTEC (2016) this system is called Chachimbiro Fault System which controls the hydrothermal alteration and hot springs found along the trace of this fault zone (Figure 5).

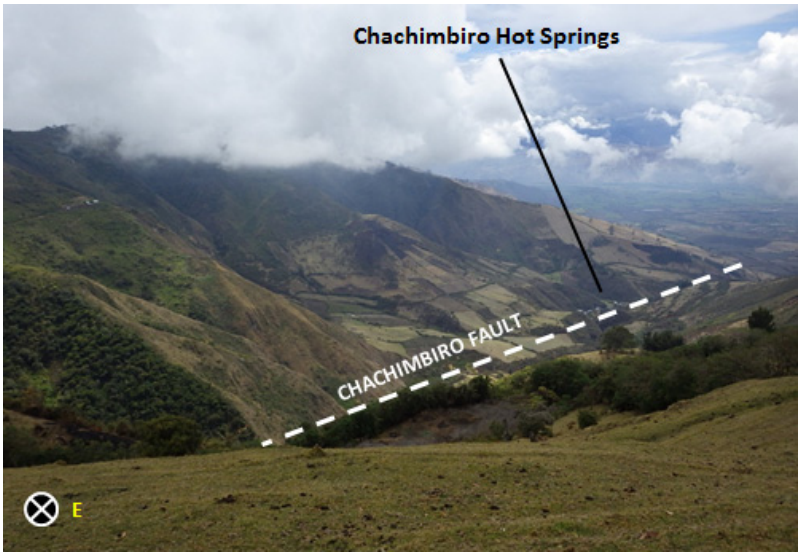

FIGURE 5: Panoramic view of Chachimbiro hot springs location and Chachimbiro Fault

3. METHODOLOGY AND DATABASE

3.1 Geology data

The geology of the Chachimbiro prospect has been mapped in detail by Ruiz G. (2011) and Granda (2011). They reviewed previous reports and interpreted aerial photographs and other remote sensing images. During the field mapping, samples were collected for petrography, chemical analysis and rock dating. Databases of the lithology information from Vallejo (2007) and Bernard et al, (2010) were the source showing the Evolution of Chachimbiro Volcanic Complex. This evolution model was presented in a technical report by SYR in 2012 and a geological map in the scale 1:25000 resulting from the fieldwork.

Analysis of structural features observed in outcrops, such as the orientations of bedding features, joints, and faults is provided by Wrightson (2011). The data set includes orientations of fault segments and fractures in the Cretaceous basements rocks as well as some specifics regarding the nature of the structural features (SYR, 2012).

Hydrothermal alteration observed in the rocks was described by Ponce (2011). During the field mapping, samples of altered rocks were collected and analysed using reflectance technology. Ponce identified six different alteration assemblages:

1) Mesothermal propylitic (chlorite-epidote-calcite); only affects the basaltic rocks and it is not associated with current thermal activity,
2) Epithermal propylitic (smectite-chlorite); associated with acid fluids and contemporaneous with the current thermal features,
3) Argillic (smectite-kaolinite); associated with hot springs and fumaroles and considered to be contemporaneous with the thermal activity,
4) Steam heated advanced argillic (opal-smectite-kaolinite); associated with fumaroles showing high concentration of H_2S, and is also considered to be contemporaneous with the Argillic alteration,
5) Carbonization; represents the deposition of carbonate minerals that form along structures where CO_2 gas is being released and;
6) Supergene advanced argillic alteration; it is not hydrothermal in origin, but rather results from the weathering of rocks.

These were mapped on a 1:10,000 scale topographic map (Figure 6).

MMC-MMTEC and CELEC EP carried out geological field work from April to July in 2016, in order to improve the geological model as the area is lacking outcrops. Several rock samples were collected in order to apply the Thermoluminescence method to characterize the heat sources, alteration zones and even doing stress modelling with new geological lineaments analysed. MMC-MMTEC identified four different alterations zones:

1) Kaolinite Zone (kaolinite ± halloysite); associated with alteration by fluids with temperatures from 100°C to 200°C. This zone covers the similar argillic area identified by Ponce (2011).
2) Steam Heat Argillic Zone (quartz ± crisobalite ± kaolinite); associated with acid fluids (H_2S) which altered volcanic rock, and this covers the same area as the steam heated advanced argillic alteration mapped by Ponce (2011).
3) Smectite Zone (smectite ± quartz ± halloysite ± Trd); extends along the Chachimbiro Fault and formed at around 130°C. This zone has been described as argillic with patches of carbonization and propylitic low-temperature alteration by Ponce (2011), but the smectite zone is covering a greater area around of Chachimbiro fault that has not been identified before (Figure 6) and;
4) Smectite Zone Discrete (Smc ± Qz); associated with regional metamorphism without any relation to geothermal fluids.

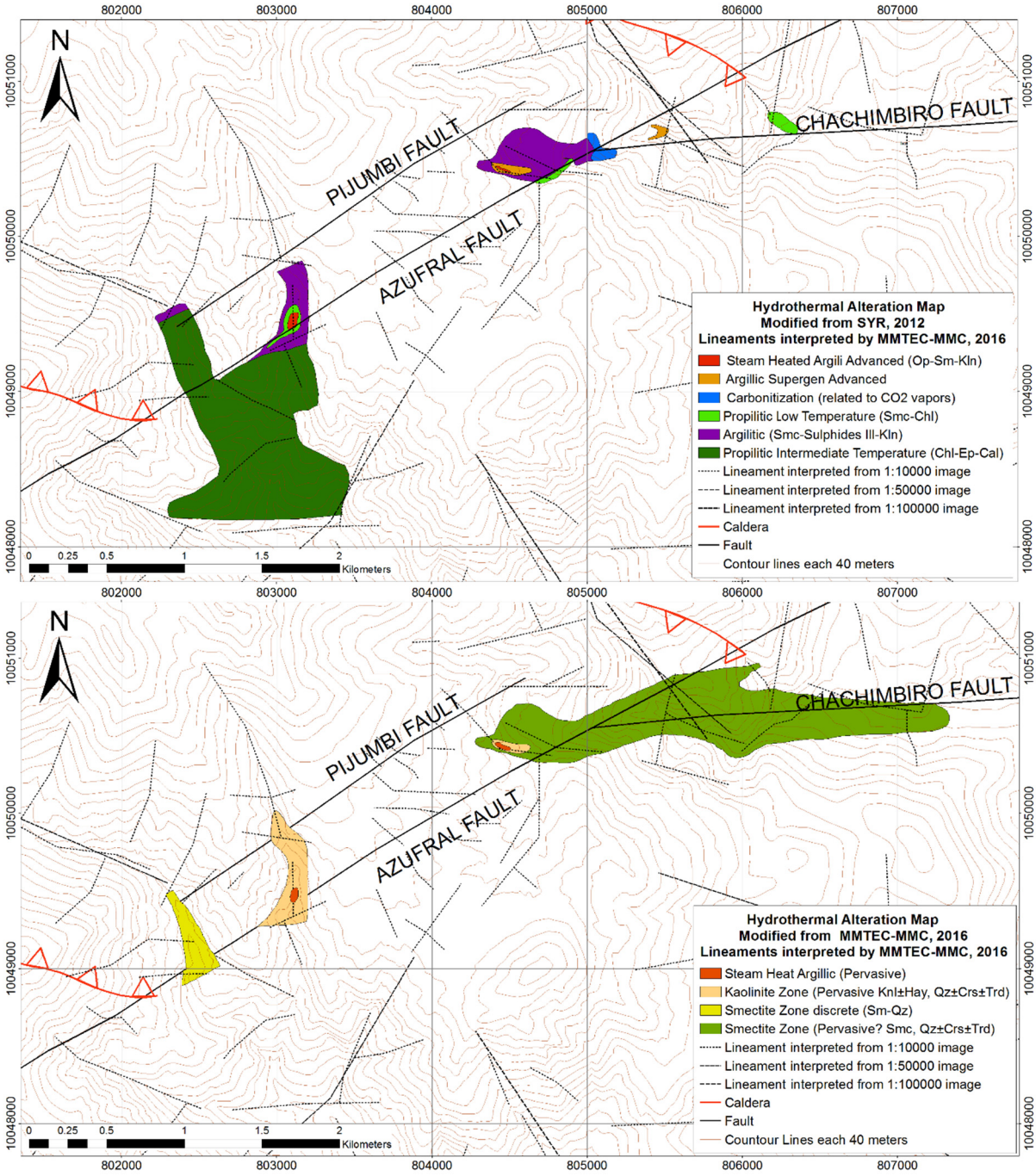

FIGURE 6: Hydrothermal alteration maps (modified from SYR, 2012 and MMC-MMTEC, 2016) which show the different zones of the hydrothermal alteration areas, except for Steam Heat Argillic Zone

All the data described above, have been provided by SYR to CELEC EP, in the form of reports and shapefile databases. In this study, these data were edited and a new dataset was generated in ArcGIS 10.3 in order to visualize the geological model in 3D using Petrel.

Geological lineaments were identified and analysed using ASTER/GDEM data and Photo-Interpretation with 1:10000, 1:50000 and 1:100000 scale by MMTC-MMC (2016) in order to locate areas with high density of lineaments and possible fractures. In this study, the data were georeferenced and plotted in order to correlate the lineaments with the main structures as well as the seismicity.

3.2 Geophysical data

Magnetotelluric data were collected in 2011 by WesternGeco Integrated EM CoE. In total 70 MT stations were installed and distributed on an irregular grid with a minimum spacing of 0.35 km between stations.

The data were processed and 1D and 3D inversions were carried out (SYR, 2012). The data were acquired as five component stand-alone remote reference MT stations with a nominal bandwidth from 0.001 to 10000 Hz. However, there are serious gaps in the survey because suitable sites were hard to find in the rugged terrain. Those gaps are northwest of Minas de Azufre, north of Timbuyacu hot spring, south of Quebrada Azufral, near MT station M33, north of Santa Susana hot spring and several locations of less conceptual interest (Figure 7).

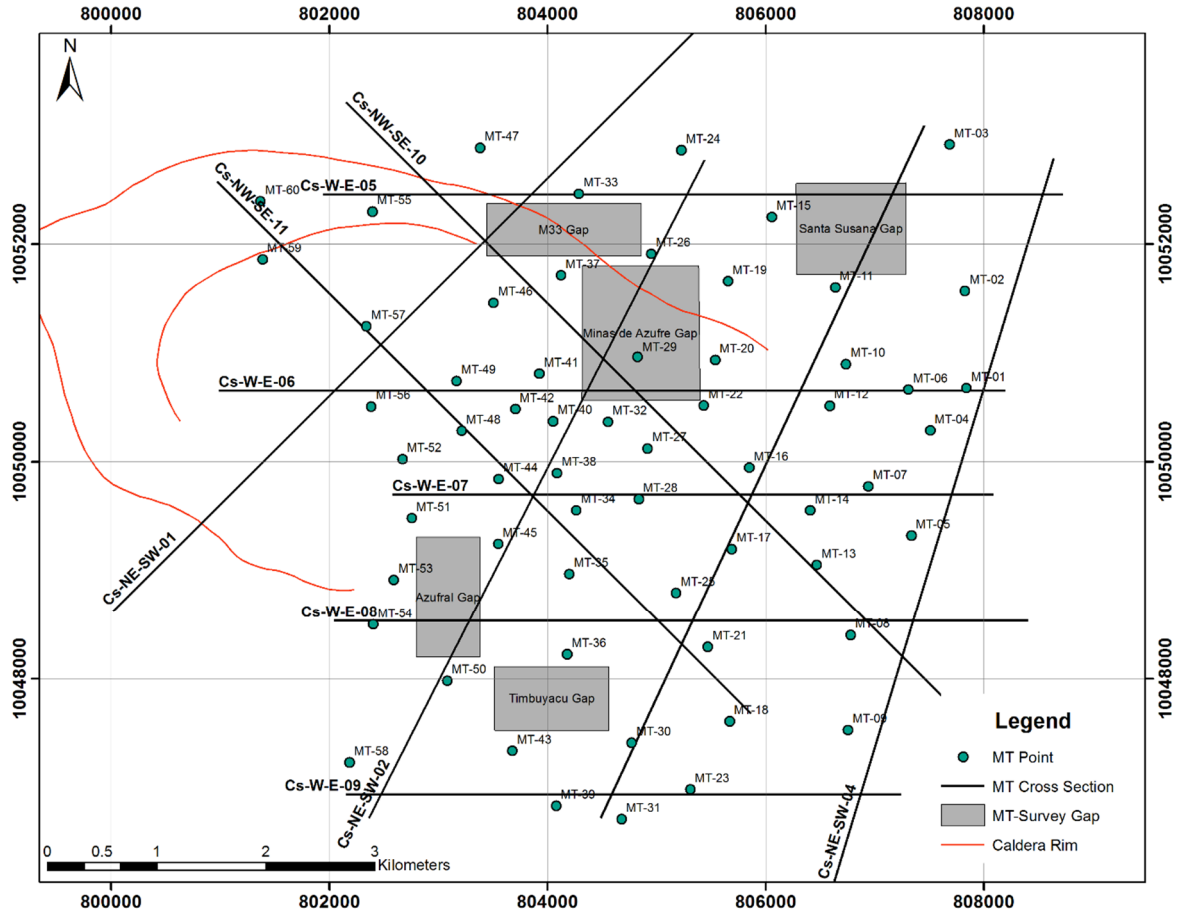

FIGURE 7: Magnetotelluric data points and cross-sections used in order to create a data grid in Petrel Software

CELEC EP has acquired a MT/TDEM equipment set which consists of six Electromagnetic Geophysical Data Acquisition Systems in order to obtain new data in the area where a low resistivity anomaly was found. These new data was collected from May to August of 2016 and are still being processed.

The present study employs eleven resistivity profiles made by Manabu Sugioka geophysicist specialist of JICA-CELEC, who is supporting the geophysical exploration in Chachimbiro Prospect. The cross-sections shown below have been selected specifically for this study (Figure 7 and Table 1- Appendix I).

The MT data were processed for Petrel analysis using ASC-II files for each cross-section. They show the resistivity values as a function of depth. In order to visualize the data in 3D, two main steps had to be performed: a) to define a grid in X, Y, Z directions and b) to populate the grid with data.

The grid was defined as a cube, which covers all cross-sections from the surface (Top Limit) to 4000 m below sea level (Base Limit). The grid increment was defined to be 50 m in the X, Y and Z directions. Petrel allows the use of several interpolation methods for computing values in cells where no data was available. In this study these methods where tested on the main input data. The Gaussian Methods show distortion in the results and do not allow to clearly define the resistivity anomalies. The Closest Method shows interpolation in data blocks and distortion at the boundaries of resistivity layers. The Functional Method shows resistivity layers with soft boundaries, nevertheless in areas with low resistivity, it shows distortion and unusual forms. The User Define Algorithm and moving average methods show intercuts with cross-sections and do not define resistivity layers.

The Kriging methods produce similar results as the approaches mentioned above. The Kriging theory conducts smoothing and exact interpolation at the same time. Further, the Kriging method makes use of a very flexible gridding scheme (Yang et al., 2004). In this study, the Kriging Interpolation Method outlined low and high resistivity layers with a minimum of distortion compared to the results of other methods, allowing us to visualize the results from the MT data in the best possible way.

3.3 Geochemical data

The Chachimbiro Geothermal Prospect consists of a number of mixed chloride-bicarbonate hot and warm springs (temperatures up to 61°C) located along Quebrada Chachimbiro in the northeastern part of the prospect area. These springs are utilized for commercial thermal spas. There are also a few hot springs at Timbuyacu (temperatures up to 41°C), on the southeastern edge of the prospect area. The Chachimbiro hot springs show the highest temperature in the prospect and appear to represent the geothermal resource waters (Table 3 in Appendix I). Sulphur gas comes up along the stream wall in local fractures, but this gas has not been sampled without air contamination.

GeothermEx, Inc participated in the pre-feasibility stage of the Chachimbiro Prospect, subcontracted by SYR in 2011, to do geochemical analysis. They designed the sampling and analysis schedule, sampled the fluids (water and gas), reviewed the lab operation and results, and compiled, integrated and interpreted the geochemistry data (SYR, 2012). The areas sampled were the Chachimbiro, Timbuyacu, Pinguchela, Pilomanchi hot springs and Quebrada Azufral gas and cold fluids (Figures 8A, 8B and 8C).

During the field campaigns, data were collected to gain information on physical (Table 3 in Appendix I) and chemical parameters (T°, pH, Eh, Ec, flow estimation). The lab results show concentrations in the order of ppm of major elements (Ca, Mg, Na, K, HCO_3, SO_4, Cl, Si and Li) and minor elements (Fe, F, NH4, B, As, Al, Cs, Rb, Br, NO_3), isotopes (δ-^{2}H, δ-^{18}O) in hot and groundwater. In addition, gas dry analysis in percentage of volume (CO_2, H_2S, NH_3, Ar, N_2, CH_4, H_2, O_2, CO) and He isotopes ($^{3}He/^{4}He$) was carried out. From these chemistry data liquid and gas geothermometers have been calculated.

GeothermEx (2011) also took into account geochemistry data published by Aguilera et al. in 2005. These data where reviewed by SYR in order to create a complete database. Aguilera (2005) also refers to the chemistry data collected by Almeida et al. (1990) which do not have geographic coordinates.

4. INTERPRETATION USING THE PETREL SOFTWARE

4.1 Structural analysis

Hydrothermal alteration is controlled by the Azufral and Chachimbiro Fault systems and NW-SE lineaments. Low emission of CO_2 and H_2S has been found in Pijumbi and Azufral faults close to the hydrothermal alteration. The gas flow and alteration disappear in Northwest direction from this point, no hot springs or gas have been found further than Pijumbi fault and Azufral stream intersection. This

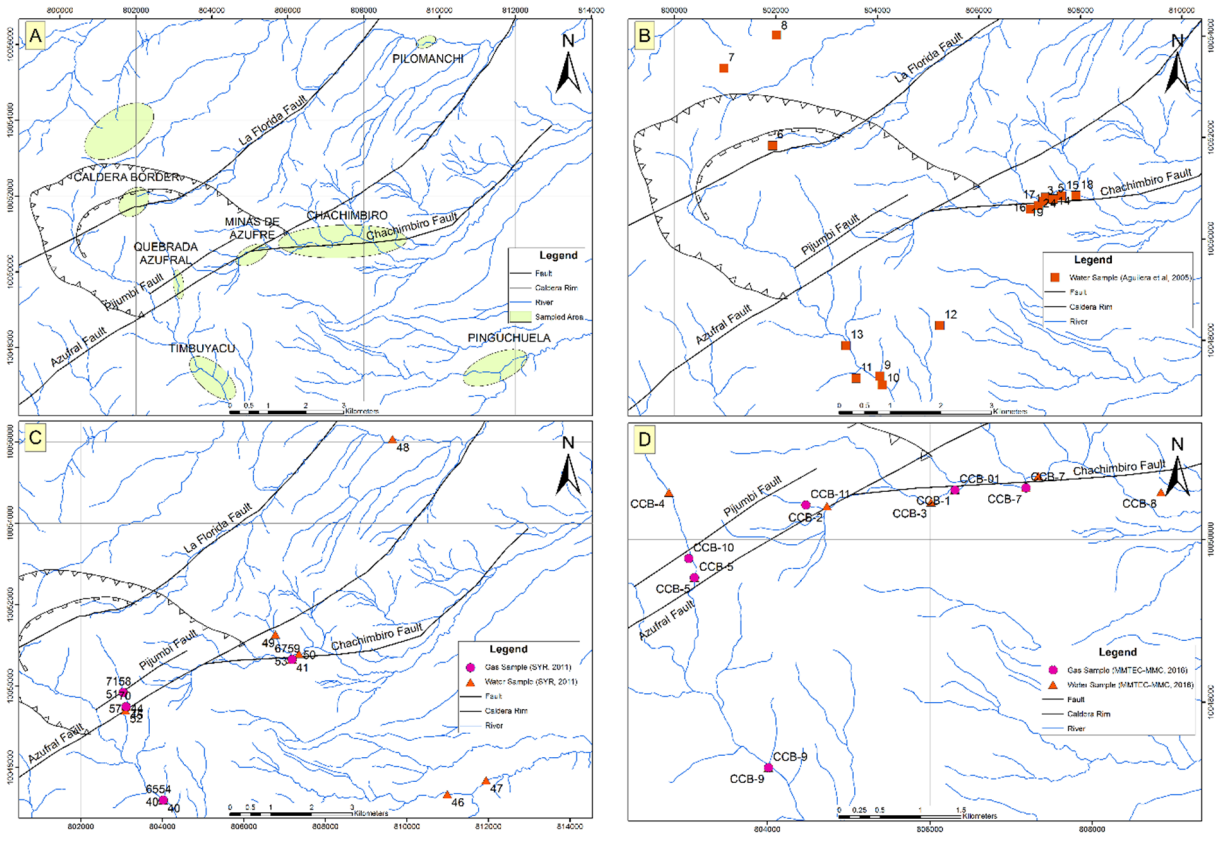

FIGURE 8: Geothermal manifestation areas (a) and area sampled (gas (b), hot springs (c) and fresh water (d)) during field campaigns in 2005, 2011 and 2016

would suggest the Pijumbi fault is a boundary of the geothermal system. Hot springs are located along the Chachimbiro Fault and the intersection with the Azufral Fault (Figure 8). This indicates that those faults control the upward movement of fluids and that the faults are permeable.

MMC-MMTEC and CELEC EP worked together and conducted a field survey from April to June 2016. The main objective was to sample gas and water at the same locations as GeothermEx (2011) and sample new hot spring locations (included Minas de Azufre gas manifestation, Figure 8D). The analysis is ongoing and some results have been shown and a preliminary interpretation has been presented by MMC-MMTEC (unpublished document). The results show the concentration of major (Na, K, Li, Ca, Mg, Cl, SO_4, HCO_3 and T-SiO2) and minor elements (NH4, AL, Fe, NO_3, NO2, F, B, and As) and isotopes (δ-^{2}H, δ-^{18}O) in water and gas dry analysis results in percentage of volume (CO_2, SO_2, H2S). In this study, the ArcGIS 10.3 software was used to create shapefiles containing the element concentration as attributes. Petrel allows shapefiles to be imported with topography information and creates surfaces that show concentration of chemical elements or temperature anomalies (see Figures 21, 22, 25 and 26 in chapter 4.3).

The quantity of lineaments increases close to the intersection between faults and alteration zones, suggesting a fracture system associated with the main structures. MMTC-MMC (2016) points out a set of W-E lineaments caused by shearing activity of the Azufral Fault at Minas de Azufre area. This also indicatesthat permeability in the system controlled by the Azufral Fault (Figure 9). There are alignment of earthquake epicentres parallel to the Azufral and Chachimbiro faults in NE-SW and E-W directions respectively. The lineaments coincide with lineaments interpreted by MMC-MMTEC (Figures 9 and 10).

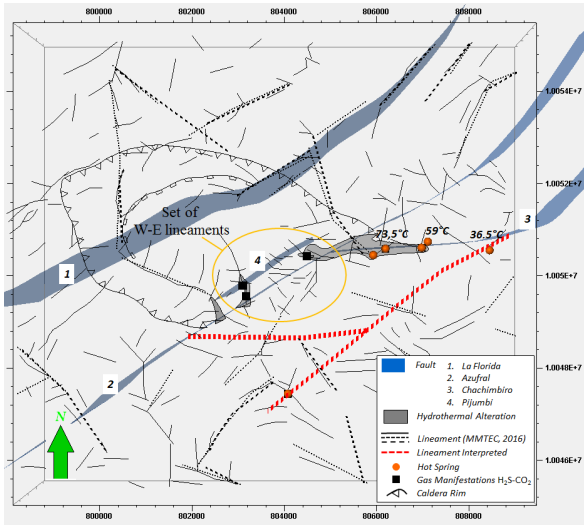

FIGURE 9: Map of interpreted lineaments that show an increase of lineaments at Azufral and Chachimbiro faults and also staggering lineaments in W-E direction in the Minas de Azufre area

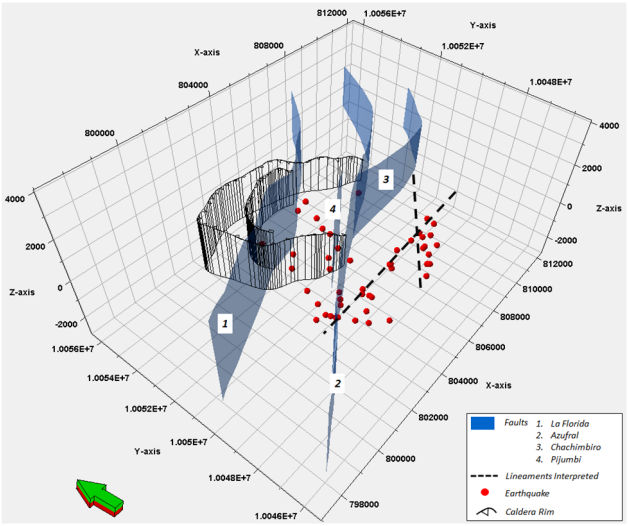

FIGURE 10: Alignments of earthquake epicentres subparallel to Chachimbiro (4) and Azufral (3) faults

The seismic activity has been recorded and the locations of earthquakes have been included into the model (Ruiz M, 2011). Figure 10 shows an alignment of earthquakes with the fault systems Azufral and Pijumbi, which confirms shearing activity.

It is important to note that in the current regional structural system, the main stress is oriented in E-W direction, which creates a subparallel fault system in NE-SW direction of the Azufral and La Florida Fault and the Chachimbiro Fault System at the same time. This interaction between faults results in a "pull apart" system in the Chacana volcanic complex (Hall, 2012). This is indicated by sub-parallel faults in the Azufral and Chachimbiro systems, which allow permeability and upward movement of fluids in the system, and also structural barriers. This strongly suggests the existence of carriers and barriers.

4.2 Magnetotelluric data analysis

Electrical resistivity is controlled by electrical properties of the material, not only related to types of rock and their composition, but also to the overall physical conditions of the media (Tikhonov, 1950 - in Sakindi, 2015). Generally, the resistivity values in a weathered layer of igneous rock from mafic to felsic composition is ranged from 3 to 300 Ωm, in clays from 4 to 100 Ωm, in tills from 50 to 2000 Ωm and in fresh water in aquifers from 3 to 100 Ωm (EOS, 2007). High permeability and porosity (fractures) increase the conductivity. This means low resistivity, which then tends to increase with depth, due to the pressure, which closes the fractures and reduces rock porosity (Palacky, 1987).

Geothermal systems show electrical resistivity (conductivity) anomalies related to clay minerals, one of the most common being smectite. The formation of clay minerals in geothermal systems depends on the temperature and chemical conditions of the fluids that flow through the rocks. A low resistivity (high conductivity) anomaly is observed on the outer and upper margins of the reservoir. The low resistivity represents the cap rock, which is underlain by a high resistivity core (Tikhonov, 1950 - in Sakindi, 2015).

Low resistivity (generally lower than 5 Ωm) in geothermal systems is associated with the smectite-zeoliote alteration zone. The resistivity increases with depth until the chlorite and epidote zones are reached, which usually forms a high resistivity core. These mineral zones also depend on temperature

conditions. The smectite-zeolite zone forms at temperatures between 50-100°C and chlorite-epidote zone forms at temperatures exceeding 250°C (Árnason et al., 2000).

To visualize the different resistivity layers in Petrel, a 3D grid was developed. Then iso-values of resistivity were generated by filtering out areas of specific resistivity. From this 3D shapes of low resistivity i.e. the distribution of the anomalies become visible. That allows the user to decide the direction of cross-sections (Figure 11). Once these have been determined, the cross-sections were completed with data previously present in the cube grid (Figure 12).

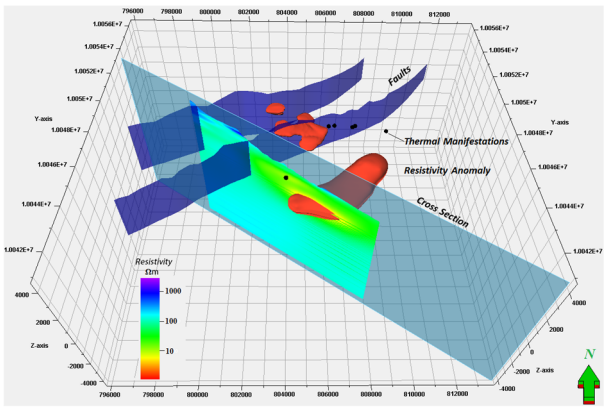

FIGURE 11: Determination process to define a cross-section in Petrel software

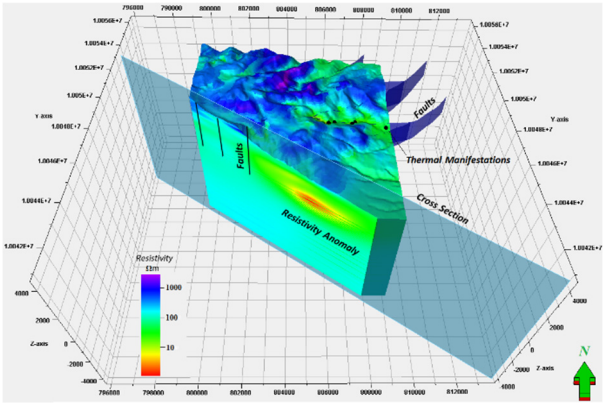

FIGURE 12: Resistivity cross-section through the cube grid populated with resistivity data

In order to visualize the low resistivity anomaly in Chachimbiro several filters were used showing different resistivity values (Figures 13, 14 and Figures 4-9 in Appendix III). Using this method, the spatial distribution of the anomalies was identified and structures and boundaries of the cap rock, and a possible reservoir, can be revealed. Table 2 in Appendix I shows the dimensions of these resistivity anomalies.

The resistivity model shows three different anomalies, two of them are large and cover extensive areas. These anomalies are separated from each other by a fault (Figure 15). The shallow anomaly, which is possibly the cap rock, covers an area of 11.07 km^2 and its average thickness is around 388 m.

In Figures 15 and 16, the low resistivity shows clear divisions of the anomaly by Azufral, Chachimbiro, and Pijumbi Fault and a division in NW-SE direction with a similar trend to lineaments was interpreted by MMC-MMTEC (2016). Another lineament in NW-SE direction has been interpreted in the borders of 5 to 7 Ωm resistivity anomaly (Figure 16). These lineaments could be fractures that increase the

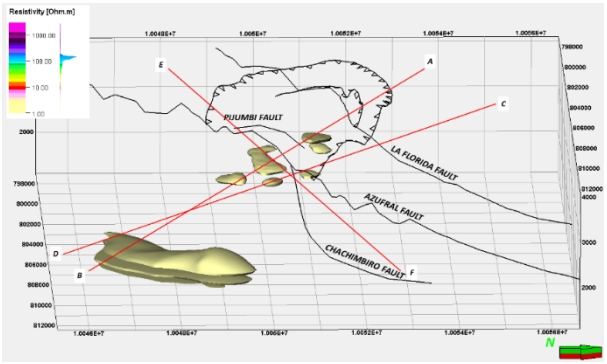

FIGURE 13: Spatial distribution of low resistivity anomalies (0-3 Ωm) and choice of cross-sections

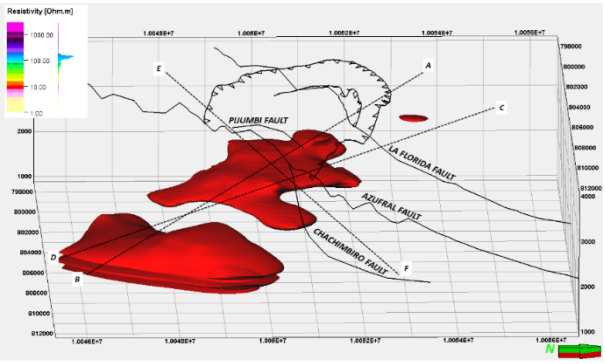

FIGURE 14: Low resistivity anomaly from 7 to 10 Ωm modelled in Petrel Software, showing its relation to faults

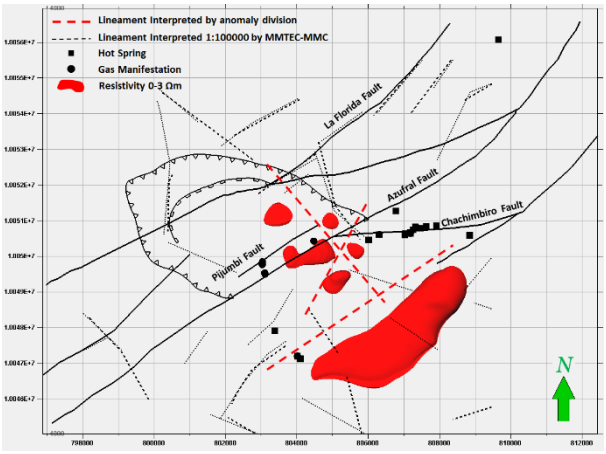

FIGURE 15: Divisions of the anomaly by Azufral, Chachimbiro, Pijumbi Fault and possible fractures in NW-SE direction

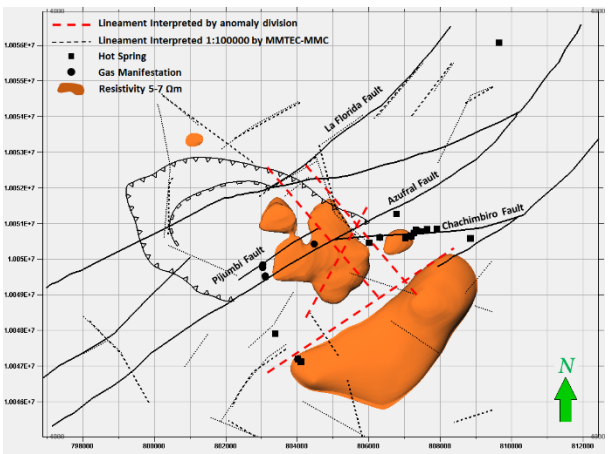

FIGURE 16: Divisions of the anomaly by Azufral, Chachimbiro, Pijumbi Fault and possible fractures in NW-SE direction

permeability of the system and outer boundaries. An important lineament has a subparallel trend to the Azufral fault that divides two resistivity anomalies (at 7-10 Ωm) and is in alignment with earthquakes, hot springs and lineaments interpreted by MMTEC (Figures 9 and 10).

Petrel can create cross-sections in any direction. Based on the analysis above, some directions of interest become apparent (Figure 13).

The resistivity distribution in Chachimbiro shows different layers. The shallow part with high resistivity (>160 Ωm) corresponds to Quaternary volcanic rocks and tills. The low resistivity zone (<10 Ωm) could be related to the cap rock, probably formed by smectite. Outcrops of smectite have been located and described in technical reports as personal documentation. Below the low resistivity anomaly, the resistivity increases gradually from 10 to 160 Ωm and forms a medium resistivity zone that includes a high resistivity core of 60 to 160 Ωm (Figures 17, 18 and 19).

Interpreted lineaments are present in cross-sections associated with earthquakes. The projection from the surface to the subsurface of Pijumbi, La Florida and Azufral faults, are aligned with hypocenter earthquakes concentration (Figures 17 and 18).

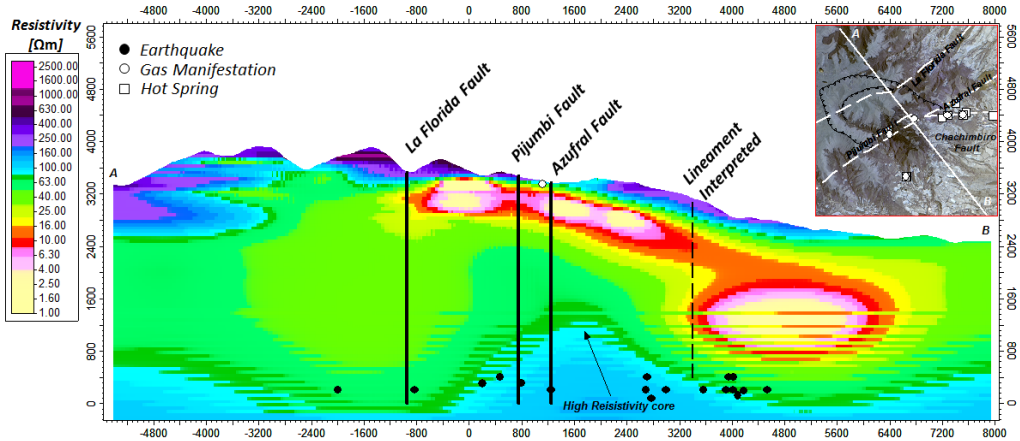

FIGURE 17: Resistivity cross-section A-B shows the high resistivity core and the relation between the interpreted lineament, earthquakes, fault, gas manifestations and resistivity anomalies

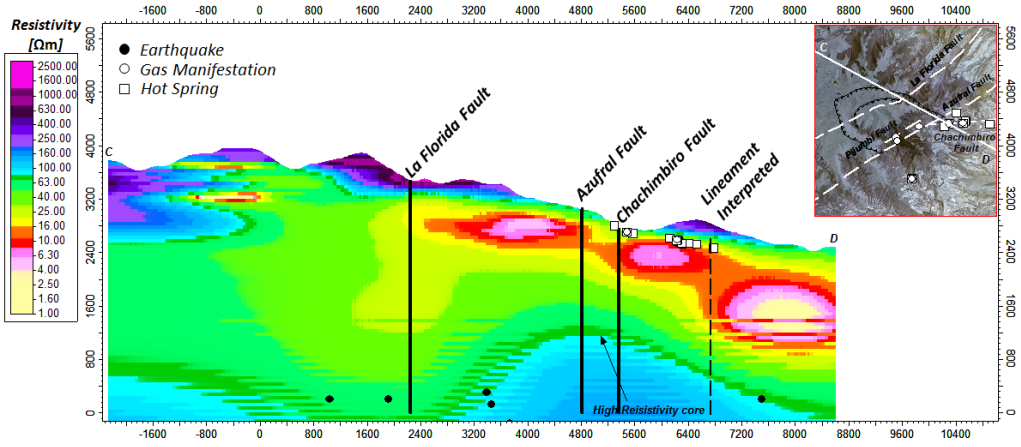

FIGURE 18: Resistivity cross-section C-D shows the high resistivity core and the relation between the interpreted lineament, earthquakes, faults, gas manifestations, hot springs and resistivity anomalies

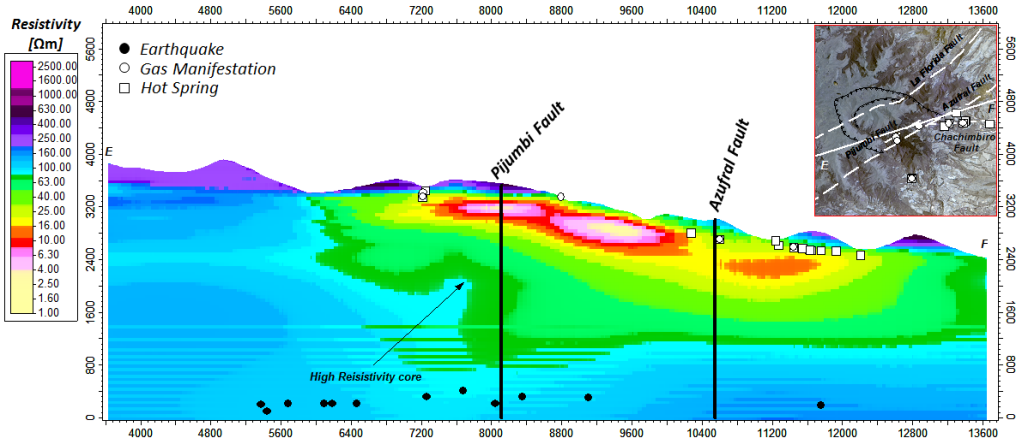

FIGURE 19: Resistivity cross-section E-F shows the high resistivity core and the relation between the interpreted lineament, earthquakes, fault, gas manifestations and resistivity anomalies

The Azufral and Pijumbi Faults are clearly affecting the low resistivity anomaly. As mentioned above an interpreted lineament (Figures 9 and 10) is also evident in the resistivity cross-sections. This inferred lineament divides the two largest low resistivity anomalies and is associated with earthquakes cutting the Chachimbiro fault and Timbuyacu valley where the hot springs are found (Figure 9 and 16).

The cross-sections show a slightly concave shape of the shallow low resistivity anomaly, which overlays a high resistivity core that is wrapped in by a medium resistivity layer (Figures 17 and 18). The faults projection from the surface to subsurface reaches the high resistivity core; hot spring and gas manifestations are located on the faults which indicates that fluids in the core are connected to the surface through the Pijumbi, Azufral and Chachimbiro Faults (Figures 17, 18 and 19).

4.3 Geochemical analysis

For the purpose of this report, the geochemistry data analysis will focus on: 1) geographical distribution of the geothermal manifestation, 2) origin of the geothermal fluids, 3) temperature of the reservoir and 4) the permeability zone.

Isotope analysis is an indispensable tool to understand the flow pattern in geothermal systems. Isotopes are sensitive to changes in temperature, water-rock interaction and other physicochemical processes, such as mixing and steam separation, and they are suitable as tracers detecting the source water and regional flow pattern.

The $\delta^{18}O$ values of geothermal waters are often higher (less negative) than those of local meteoric waters, an oxygen isotope shift has been termed in the diagram $\delta^{18}O$-$\delta^{2}H$. This has been interpreted as the result of isotopic exchange at high temperatures between the water and the rock (Abaya et al, 2000).

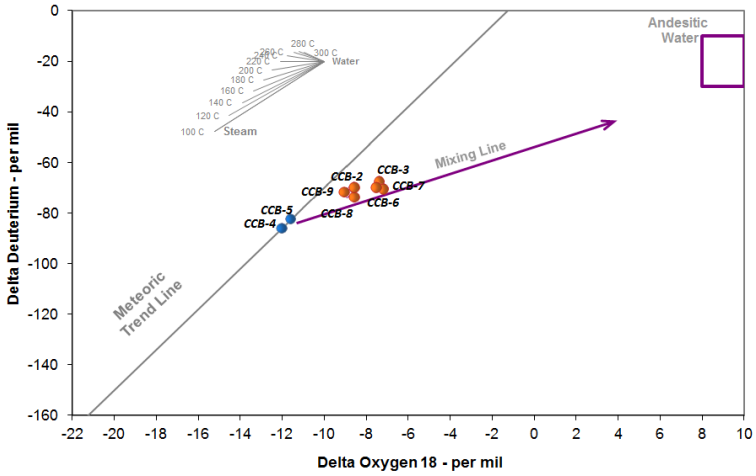

FIGURE 20: Diagram $\delta^{18}O$ - $\delta^{2}H$, applied to the Chachimbiro water samples

Figure 20, shows that the Azufral water samples (CCB4 and CCB-5) are on the local meteoric trend line. These samples are cold groundwater with rock interaction at subsurface collected next to the CO_2 and H_2S gas manifestations. The hot spring samples (CCB-1, CCB-2, CCB3-CCB-6, CCB-7, CCB-8, CCB-9) in Chachimbiro and Timbuyacu areas show an oxygen isotope shift and these samples are almost in the same value range as the $\delta^{2}H$ isotope. That implies that these hot springs are of meteoric origin with subsurface rock interaction (Abaya et al, 2000).

Figure 20 also shows a mixing line trend to the andesitic water. That indicates input of andesitic water to the geothermal system from significant depths and mixing with geothermal fluids. Nevertheless, the oxygen isotope shift is normal compared to meteoric waters and the possibility of input from andesitic water to the geothermal system is minimal.

Geothermometers and isotope analyses probably constitute the most important geochemical tool for the exploration phase. Geothermometry is used to estimate subsurface temperature. During the ascent of geothermal waters from a deep reservoir to the surface, they may cool by conductive heat loss as they travel through cooler rocks or by boiling as the hydrostatic head decreases. When geothermometers are applied to measure subsurface or aquafer temperatures, basic assumptions are always made, namely that the temperature dependent chemical or isotopic equilibrium prevails in the source aquifers (D'Amore and Arnórsson, 2000).

SYR (2012) developed three different scenarios for Chachimbiro system based on geothermometer temperature:

1) The first model is a moderate temperature hydrothermal system with neutral chloride reservoir water at 225-235°C and deep temperatures as high as 260°C. It is based upon the neutral chloride chemistry of the hot springs, temperatures predicted by the Na-K and CO/CO2-CH4/CO2 geothermometers.
2) The second model is that of a low temperature (110-125°C) formation water, referred to as "immature water", based upon predictions of the K-Mg and sulphate isotope geothermometers.
3) The final model is that of a cooling magma-hydrothermal system, with temperature of 110-125°C, supported by carbon and helium isotopes.

This report shows the temperature in the subsurface based on liquid geothermometer and using the chemical data collected by MMC-MMTEC (2016). The analysis of the results can be found in Table 5 in Appendix I and Appendix II. The chemical data were processed with Plotting Spreadsheet developed

by Powell and Cumming in 2010. Only four samples could be used for the next analyse described below because some samples are out-of-ionic balance between anions and cations (Table 4 in Appendix I). The Na and K cations usually are in high concentration in deep areas in the reservoir and they are only in low concentration in meteoric water. Thus, the Na/K ratio does not change even when there is a mixing process between hot and cold water. The geothermometers that use Na and K cations are the best for fluids derived from a thermal environment (> 180°C), and also the flow rate of a spring may be less than is required for the application of the quartz geothermometer (Yock, 2009). The highest temperature based upon Na/K geothermometers is around 285°C (Tonini, 1980), but the average value is 240°C. These values are close to the temperature values reported by SYR (2012) in their first model, which is related to neutral chloride reservoir water.

The Na/K geothermometers are applicable in Chachimbiro geothermal system and the values calculated using those methods were used to create temperature iso-lines at different epochs in Petrel Software (Figures 21 and 22). Figure 21 shows core temperature areas of over 300°C. This anomaly covers Minas de Azufre, Quebrada Azufral and partially the intersection between the Chachimbiro and Azufral faults. The figure also shows an area with Na/K temperature less than 200°C that overlaps with the hydrothermal zone. Figure 22 shows high temperatures (from 250 to 300°C) next to Minas de Azufre area and here also the most extensive hydrothermal alteration area, which overlaps with the 250°C temperatures area, can be found. There is a slight correlation between the two iso-lines graphics (Figures 21 and 22). The main reason may be due to the distribution of the samples and also, the methodology used to obtain the temperature values with the K/Na geothermometer. However, it seems that the high temperature area overlaps with the large alteration zone and also the Azufral area (Figures 21 and 22).

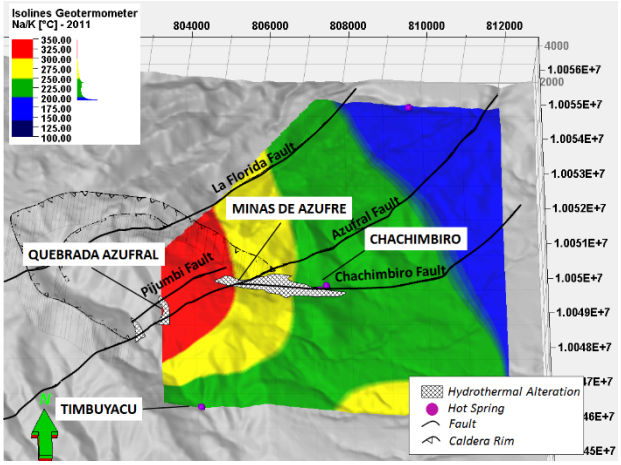

FIGURE 21: Isolines based on temperatures obtained with K/Na Geothermometer, using ion concentration from hot spring samples collected by GeothermEx in 2011

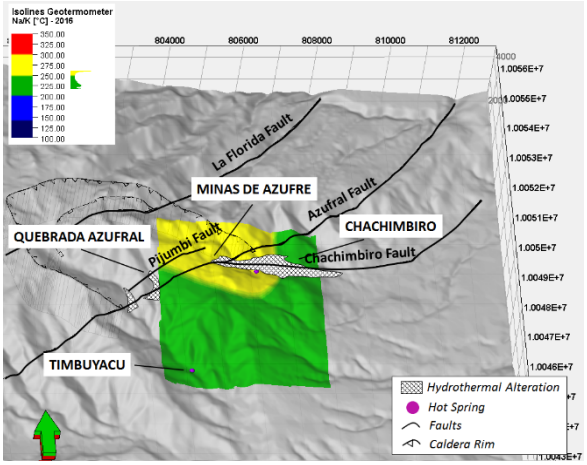

FIGURE 22: Isolines based on temperatures obtained with K/Na Geothermometer, using ion concentration from hot spring samples collected by MMC-MMTEC in 2016

The permeability can be interpreted with direct observations in the field and analysis of the distribution of the fluids at the subsurface. In the Quebrada Azufral and Minas de Azufre area there are several gas manifestations of CO_2 and H_2S at low flow rate and pressure. These are located on the stream bedrock (bubbling gas, Figure 23) and also in fractures on the stream walls, where native sulphur precipitates (Figure 23). These emissions are controlled by the Azufral fault that also controls the hydrothermal alteration in this area. It is important to mention there are no hot springs in the area.

The hottest springs are located along the Chachimbiro Fault in Chachimbiro area. These hot springs precipitated $CaCO_3$ and there is no emission of H_2S. Most of the hot springs are entrapped in cement boxes which feed the Chachimbiro spa (Figure 24). The Timbuyacu hot springs appear not to be related with any structures.

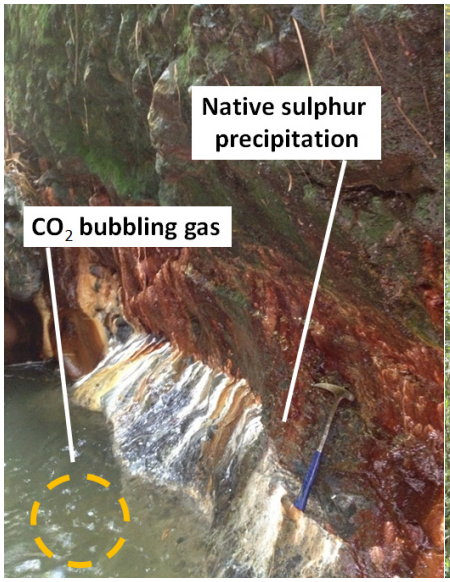

FIGURE 23: CO_2 emission on the bedrock stream at Quebrada Azufral area and Native Sulphur precipitation on fractures

FIGURE 24: Hot Springs entrapped in cement box at Chachimbiro area

The higher concentration of hot springs at Chachimbiro shows that the most permeable area is related to the Chachimbiro fault. Permeability is also related to the Azufral fault where CO_2 and H_2S indicate a degasification zone at depth.

The temperature iso-lines in Figures 25 and 26, show the Chachimbiro area as the hottest point at the different epochs, as might be expected. From Chachimbiro the high temperature trends to the North, Southeast and Southwest. The iso-lines do not represent the temperature gradient; the rock is not an isotropic environment and the iso-lines have been interpolated based on hot spring temperatures. However, it may represent a main zone of outflow such as Chachimbiro area and lateral outflows such as Timbuyacu, Pinguchuela and Pilomanchi.

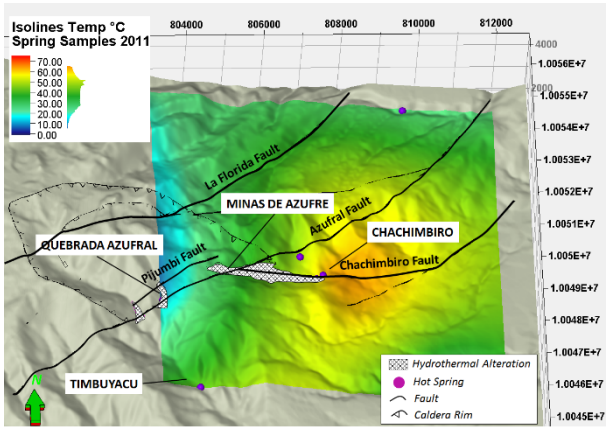

FIGURE 25: Isolines based on hot spring temperatures measured by Geothermex (2011)

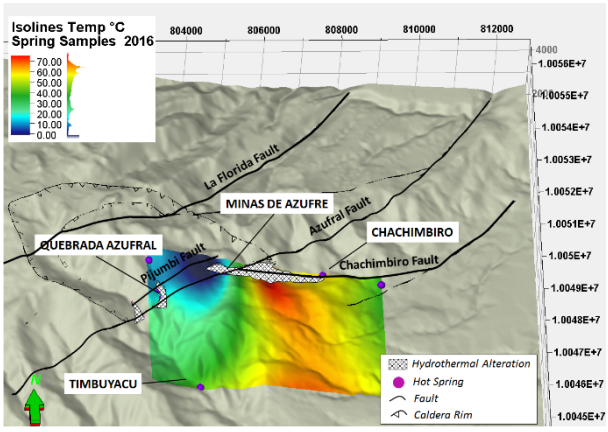

FIGURE 26: Isolines based on hot spring temperatures measured by MMC-MMTEC (2016)

5. GEOTHERMAL MODEL OF CHACHIMBIRO IN PETREL

The available data for the Chachimbiro geothermal prospect has been described in previous chapters. In this chapter, a conceptual model is presented. This is an early model so it is simple and based on analogies with geothermal fields that are better understood. When a resistivity survey and other surveys such as geochemistry are done, the outline of the field can be defined approximately, and geothermometers can indicate a possible reservoir temperature. After that a very simple model could yield an estimate of the potential power-generation capacity (Lumb, 1981).

Axelsson (2013) mentions the information from the geothermal systems that should be incorporated in a conceptual model. His method is applied for describing the Chachimbiro system making use of the available information. This study uses his guidelines and takes into account that not all geothermal conceptual models incorporate all the components.

5.1 Estimate of the system size

The sizes of geothermal systems worldwide tend to follow a log normal size distribution. In Chachimbiro there is considerable uncertainty concerning boundaries, temperatures and thickness. This study defines the boundaries using the dimensions of the low resistivity anomaly as the areal extent. This could be interpreted as the largest possible area of a resource. New geological, geochemical and geophysical data are under revision by MMTEC and MMC (2016) which will provide information about the size of the system and will also complement borehole information of scheduled drilling projects. Currently, the areal extent of the system is believed to be 11.06 km^2 based on the low resistivity anomaly (between 0-10 Ωm) and the thickness is about 3400 m from the surface to where the possible up-flow is located (resistivity anomaly 90 Ωm).

5.2 Nature of the heat source(s)

SYR (2012) suggests that the heat source is located near the Huga dome (Figure 27). This is indicated by its volcanic history (emplacement occurred 30.000 years ago) and composition (rhyodacite). These domes are interpreted as magmatic intrusions, and these have been controlled structurally by the La Florida fault (Figure 27). Bernard et al. (2014) documented volcanic activity between 3640 and 3510 years BC, which extruded a ~650-m-wide and ~225-m-high rhyodacite dome, located 6.3 km east of the magma chamber which is emplaced at two different depths (~14.4 and 8.0 km). The hot (~940°C) deep reservoir fed the central vent while the shallow reservoir (~860°C) had an independent evolution controlled by regional faults. This indicates partial migration of the heat source to the East, located below the Chachimbiro dome (CH4) at shallower depths (Figure 27).

The resistivity records show two high-resistivity anomalies of >150 Ωm (Figures 1 and 2 in Appendix III); one of them is under the Albují and Hugá (CH3) domes and the other is under the Chachimbiro emission centre (CH4). These anomalies could relate to two intrusions, which are the heat source of the system (Figures 1 and 2 in Appendix III) and this also corresponds to the model by Bernard et al. (2014) suggesting that two different magma chambers exist. Figure 28 shows the 3D model of Chachimbiro, and it shows a clear structural control over the magma ascent. The evidence of the magma at surface is the Albují and Hugá domes. However, the high resistivity anomalies have been modelled by extrapolation in sectors where MT data is missing. In order to strengthen this model, gaps in gravity and seismicity data need to be closed.

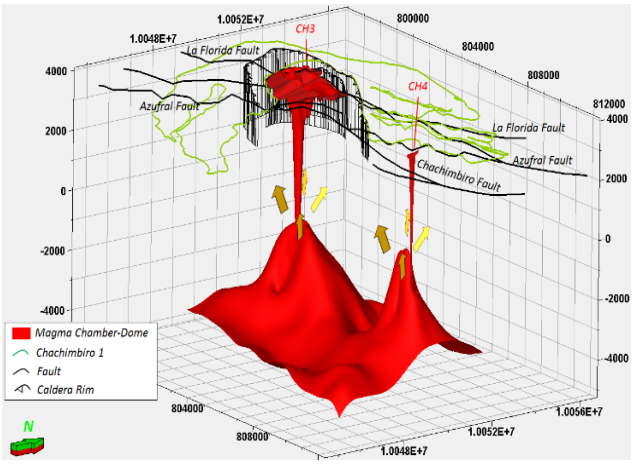

FIGURE 27: Magma intrusions that function as a geothermal system heat source and fed the emission centre in Chachimbiro volcanic complex

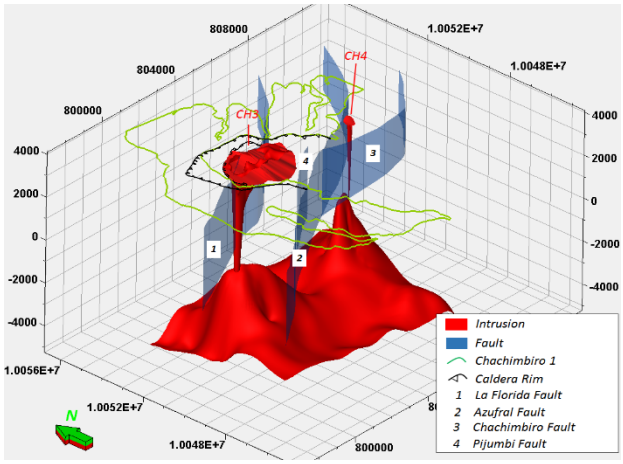

FIGURE 28: Structural control by La Florida Fault about magma rise that form Albují and Huga domes (CH3)

5.3 Location and strength of the hot up-flow/recharge zones and origin of the fluid

The $\delta^{18}O$ and $\delta^{2}H$ isotopes show a clear meteoric origin of the water in the hot springs of Chachimbiro (Figure 20). The geological structures allow the infiltration of the rain-ground water into the subsurface where it is heated up by convection and then rises to the surface where it forms hot springs in the Chachimbiro area.

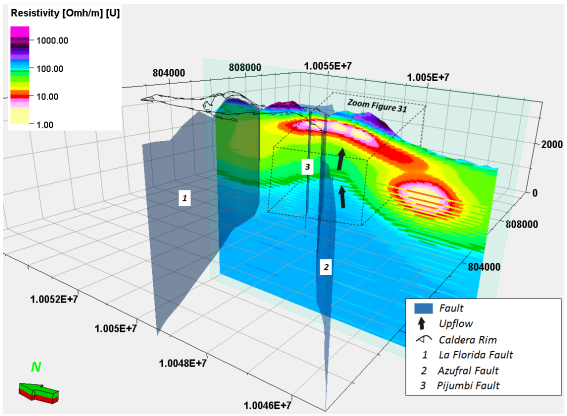

FIGURE 29: Up-flow controlled by the Azufral Fault

The low resistivity cap partitions the geothermal field hydrology into a shallower cooler meteoric zone and a deeper high temperature zone because the low resistivity (lower than 5Ωm) is associated with cap rock composed of clay, which has low permeability (Árnason et al., 2000). This cap rock covers a geothermal reservoir and accumulates heat by trapping the buoyant thermal up-flow. The up-flow zone is the reservoir zone in which flow is predominantly vertical and temperature generally increases with depth (Cumming, 2009). This means, in this case, that the up-flow in Chachimbiro is located where the high resistivity core is identified, beneath the cap rock and is apparently controlled by the Azufral Fault (Figure 29).

5.4 Location and strength of colder recharge zones

Marginal recharge represents the influx of cooler marginal meteoric waters into the geothermal reservoir. Cooler water can flow into a geothermal up-flow zone through permeable channels, from either side of the system if the groundwater has more pressure than the reservoir. It may also enter from overlying aquifers at higher elevations (Cumming, 2009).

The Chachimbiro volcanic complex is covered by the Páramo area (Andean ecosystem) which absorbs and percolates 600-1000 mm/year of rain water at more than 3000 m elevation (Hofstede et al., 2014). The river system shows several hydrography sub-basins outlined by geologic structures that both border

and exist inside the volcanic complex (Figure 3 in Appendix III). SYR (2012) documented a fracture zone that borders Caldera-1, lava flow fractures and contact zones, flow foliation in the dacite domes, contact zones between individual domes, and vertical fractures bordering the dome feeder dikes. These structures and lineaments will allow part of the groundwater to enter the host rock of the geothermal resource.

5.5 General flow pattern in the system in the natural state and changes in the pattern induced by production

As mentioned before, the low resistivity anomaly often correlates with more intensely altered up-flows. The steam dominated geothermal reservoirs are usually sealed by mineral alteration (smectite), with fumaroles, sinter, ± mud pots and high flow of non-condensable gases such as CH_4, H_2S, CO_2, H_2 and N_2. Water dominated reservoirs usually have outflow zones where buoyant hot water flows up through tabular aquifers under the smectite cap rock, without fumaroles, sinter and mud pots. The outflow is predominantly horizontal and temperature declines with depth underneath the main outflow zone (Cumming, 2009). In natural state, Chachimbiro geothermal system is dominated by liquid phase (there are no fumaroles, mud pots and low flow of non-condensable gases at surface).

In the reservoir and the core, the fluids are in convection due to the interaction between hot/basal recharge from a magmatic chamber and fluid meteoric water that percolates through open structures (see cold recharge zones in section 5.4). The geothermal fluids are accumulated beneath the cap rock, which is interpreted as the low resistivity anomaly, due to thermal buoyancy. There is no chemical evidence for magmatic fluid input. The outflow is stablished through the system faults. This is indicated by several hot springs and gas manifestation located on top of faults that bound the low resistivity anomaly. It suggests the existence of a subsurface connection between the upflow zone with the Chachimbiro area (hottest spring) and the Azufral and Pijumbi Fault (gas manifestations). The Timbuyacu springs do not have a structural connection to the upflow zone which is the outermost zone. It can be explained as a lateral discharge of the system through hidden structures. The Pilomanchi and Pinguchuela hot springs show lateral discharge that has been mixed with ground water, as indicated by their low temperatures (24.8 and 30°C) and high concentrations of magnesium with regard to Chachimbiro hot-springs (Figure 30).

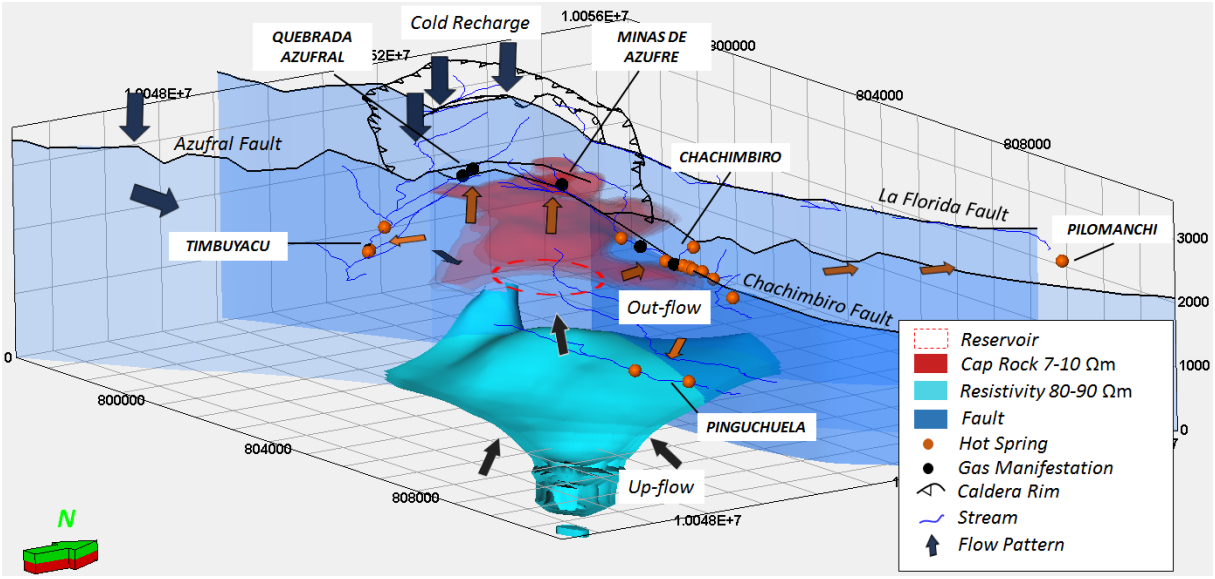

FIGURE 30: Flow pattern of fluids (perpendicular view to the main faults) that shows the cold recharge areas at the Chachimbiro highlands (Caldera Rims and Domes and the upflow zones beneath of cap rock (high resistivity)

5.6 Temperature in the system

For the purpose of this study, the temperature can be estimated by two methods. The geothermometer Na/K ratio in samples which where collected in 2016 shows temperatures of around 240°C. SYR (2012) reports temperatures of about 260°C in their first model. The resistivity method shows an increase in resistivity beneath a low resistivity layer. However, the resistivity method indicates that the maximum temperature that was reached in the past and does not reflect the current temperature of the system.

In many high temperature geothermal systems the transition between low to high resistivity anomaly core corresponds to a mixed clay/chlorite zone. Underneath the resistivity increases again considerably and stays relatively high in the chlorite and chlorite-epidote zones at temperatures exceeding 250°C (Árnason et al., 2000).

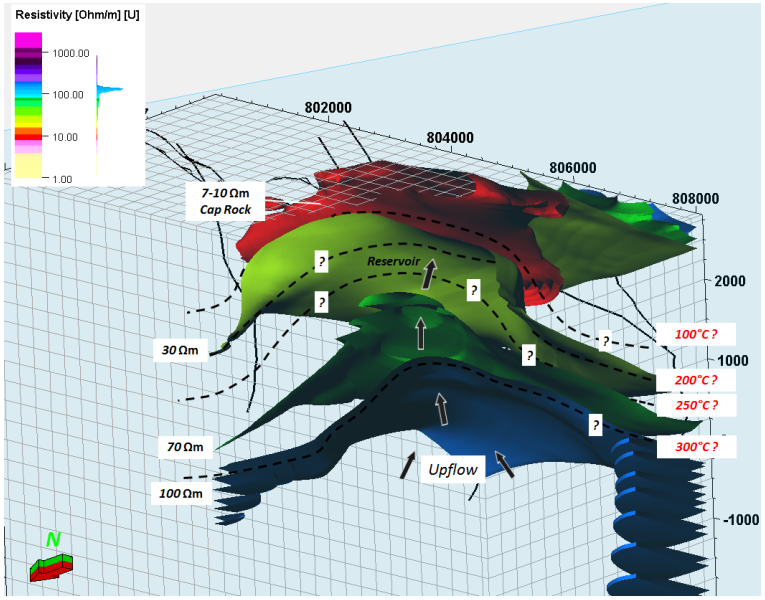

FIGURE 31: The isotherms in the Chachimbiro Geothermal System sketched based on guidelines given by Árnason (2008) and Cumming (2009)

Figure 31 shows a sketch based on the Chachimbiro resistivity maps and geochemical data following the conceptual guidelines given in Árnason et al., (2000) and Cumming (2009). Given the mapped alteration in the area, the shallow red zone (<10 Ωm) is likely to be a hydrothermal smectite clay cap. To reconcile the chemistry of the surface manifestations with the existence of a >240°C neutral geothermal reservoir, an intermediate aquifer that leaks to the surface has been assumed, which flows and carries the hot water to the permeable Chachimbiro fault where the hot springs rise to the surface.

5.7 Location of main permeable flow structures

The permeable structures in the Chachimbiro area are where the hot water rises to the surface and forms hot springs. The Chachimbiro fault controls the ascent of water in the area. The fault is E-W trending, and is limited by the Azufral fault and crosses the low resistivity anomaly (cap rock). The Chachimbiro fault seems to control the flow from the reservoir to the surface. The Minas de Azufre and Quebrada Azufral areas show hydrothermal alteration (smectite) in outcrops related to the cap rock as indicated in the magneto-telluric model. In these areas, only CO_2 and H_2S emission with low pressure are present in fractures. In these areas, lower permeability can be interpreted compared to Chachimbiro Area, and they are also controlled by the Pijumbi and Azufral faults. It is important to point out that the H_2S and CO_2 emission indicate volcanic activity in the subsurface but not an active geothermal system. The main signal of the geothermal system in Chachimbiro area is the presence of hot springs (Figure 32).

5.8 Delineate of cap-rock in the system (horizontal and vertical boundaries)

The Chachimbiro system has a horizontal boundary (cap rock) which is defined by low resistivity (0-10 Ωm) and is identified using interpolation of magnetotelluric data in the Petrel software (Figures 14, 17,

18, 19, 30, 31 and 32). The cap rock forms an irregular shape that covers 11 km^2 and its thickness is ~340 m. Possibly, the low resistivity cap rock corresponds to temperatures in the range of 50-100°C, depending on the intensity of the alteration. The transition from the low resistivity cap to the highly resistive core corresponds to temperatures in the range of 230-250°C (temperature interpreted based on high temperature geothermal systems surveys), where the reservoir would be emplaced. The horizontal natural boundaries are the Chachimbiro, Pijumbi and Azufral faults, which controlled the hydrothermal alteration in the past and still control the current raise of geothermal fluids to the surface. These structures partially enclose the cap rock in the north (Chachimbiro Fault) and cross cut the middle of the cap rock (Pijumbi and Chachimbiro). However, such enclosing geological structures have not been recognised in the south and east. Figures 7 and 8 show lineaments based on earthquakes epicentre alignments and anomaly divisions that could enclose the system; nevertheless, this should be confirmed by gravimetric and seismic data.

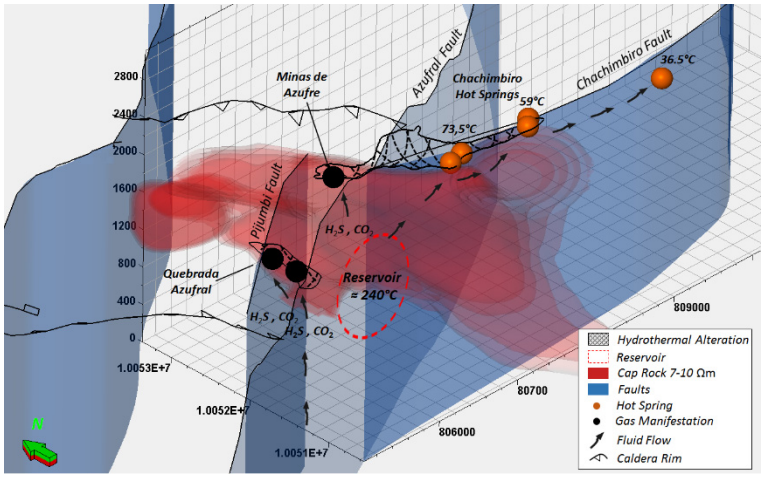

FIGURE 32: High permeability in Chachimbiro area. Hot springs are controlled by the Chachimbiro fault and low permeability at Azufral Quebrada and Minas de Azufre are controlled by the Azufral and Pijumbi faults

Axelsson (2013) mentions other components in the geothermal systems such as pressure in the system, locations of phase zones, as well as steam-dominated zones and division of systems into subsystems. The Chachimbiro project is in the surface exploration phase (preliminary study as described by Steingrímsson (2009), meaning there are no boreholes in the area. Therefore, there are not enough data available to describe all the components of the model.

6. DISCUSSION AND PROPOSAL WELL

The geothermal models of Chachimbiro area have been presented by Aguilera (2005) and SYR (2012) using surface database. They conclude that the Chachimbiro geothermal area has a small to moderate size resource with high temperature to an immature system (the geothermal fluids have not reached the chemical equilibrium) in a cooling phase, based on of the resistivity anomaly area and the geothermometers. New geochemistry data collected by MMC-MMTEC (2016) have been analysed in this report and the results are not different from SYR (2012) (reservoir temperature ~240°C). For this report the resistivity data collected by SYR (2012) was modelled using Petrel and the area extent is also comparable (11 km^2 to 12 km^2 reported by SYR in 2012). Thus, the Chachimbiro prospect should enter the exploratory drilling phase. Then the question is: Where should the first well target be located? Geothermal systems in the world have been exploited where at least two parameters (temperature and permeability) are sufficiently high. In Chachimbiro, these parameters have been in continuous discussion. Nevertheless, the only way to confirm the geothermal resource is the drilling of an exploration well.

SYR (2012) proposed to first drill a vertical well (slim hole) at location 803500E/10049900N in the WGS 84-17N (Figure 33) system. This is based on the assumption that the Azufral fault has a slight dip to the SE, and it controls the permeability in the system as well as on accessibility to the area. This point is located between the Azufral and Pijumbi faults which could ensure sufficient permeability. The well

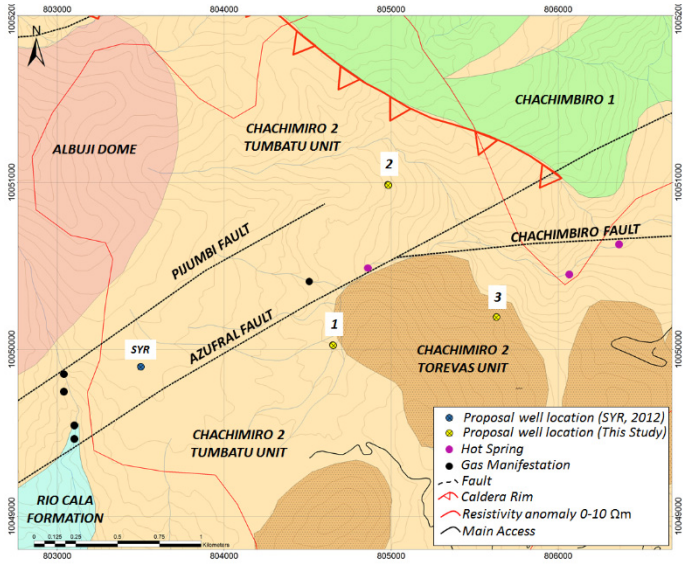

FIGURE 33: The proposed locations to drill the first geothermal well in the Chachimbiro prospect

would infuse the 7-10 Ωm resistivity anomaly until it reaches the 30 Ωm resistivity anomaly, which correspond to 200°C. However, this point is on the edge of the anomaly.

The present report suggests well targets based on the permeability given by the interaction between faults, their relation with hot springs and gas manifestations, the largest hydrothermal area, the anomaly temperature by geothermometers, the possible cap rock indicated by low and high resistivity anomalies and also the suggested upflow zone. The first target is the intersection between the Chachimbiro and Azufral faults, which is covered by the cap rock and could give more permeability to the system. The second target is the Chachimbiro fault, which is apparently the most permeable area. This fault controls the upflow of the hottest water to the surface. Three different locations are proposed to access these targets (Figure 34).

The first proposed location is in the centre of the low resistivity anomaly (804650E/10050000N in WGS 84-17N) and beneath the high resistivity core where the upflow is located. The permeability in the sector would be controlled by the Azufral fault and the 30 Ωm resistivity anomaly (possibly 200°C) at 900 m depth and 70 Ωm resistivity anomaly (possible >250°C) at 1780 m depth would be reached.

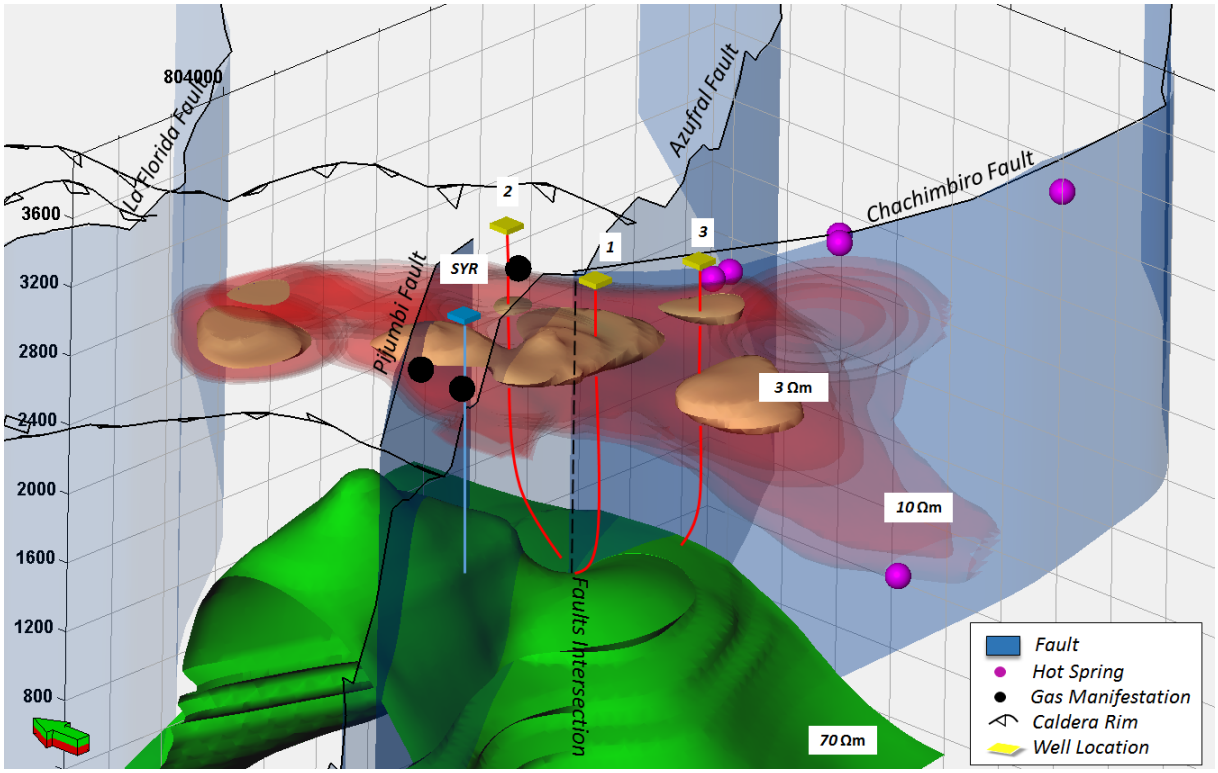

FIGURE 34: Proposed locations for the drilling of the first geothermal well in Chachimbiro prospect using Petrel

The second proposed location is at the northern border (804970E /10050950N in WGS 84-17N) but the permeability in this sector is controlled by an interaction between the Azufral and Chachimbiro faults. This location reaches the 30 Ωm resistivity anomaly (possibly 200°C) at ~1100 m depth and the 70 Ωm resistivity anomaly (possibly >250°C) at 1940 m depth.

The third is located on the opposite side of the drill point which was proposed by SYR (805600E/10050200N in WGS 84-17N), but it is closer to the resistivity anomaly centre. The permeability in the sector is controlled by the Azufral and Pijumbi faults. The 30 Ωm resistivity anomaly (possibly 200°C) is reached at 950 m and the 70 Ωm resistivity (possibly >250°C) at 1750 m depth.

The first two options are directional wells for the purpose of cutting the intersection of two faults and the third which is also a directional well that should cross the Chachimbiro fault. These wells should extend down to around 2000 m depth, where the supposed reservoir is located (Figure 34). These drill sites have been selected without consideration of road access, protected areas, relief or settlements.

7. CONCLUSIONS AND RECOMMENDATIONS

Petrel is a convenient tool to model geothermal systems. It allows the visualization in 3D including all surface data that have been collected so far to support previous interpretations as well as creating new interpretations.

Interpreted lineaments and faults are lateral boundaries of the system, which locally limit the pathways of the natural discharge of the system. However, it is necessary to correlate these interpretations with gravimetric data. A magma chamber feeds the main and lateral emission volcanic centres in Chachimbiro and is at the same time the heat source of the system. Nevertheless, the location of this magma chamber has to be confirmed with gravimetric and new passive seismicity data.

The low resistivity layer (0 to 10 Ωm) is interpreted as cap rock which covers the alleged reservoir. The resistivity model forms a concave shape where the up-flow could be emplaced. The Na/K liquid geothermometers are the most applicable in Chachimbiro are and these show temperatures of around 240°C in the reservoir. This is consistent with the resistivity layers between 30 to 70 Ωm (possible 200°C to 250°C). However, the Chachimbiro hot springs show poor equilibrium with the rock and the resistivity anomalies could not represent the current temperature in the system.

The inflow in the system consists of cold recharges from the highlands in Chachimbiro area. This cold recharge of meteoric water (isotopic evidence) interacts with the up-flow under the cap rock and forms a possibly liquid dominant reservoir. The surface expressions of this reservoir are the gas manifestation in the Quebrada Azufral and Minas de Azufre areas (low permeability) and the hot springs in Chachimbiro Area (high permeability). Lateral flow discharges are located in Timbuyacu, Pinguchuela and Pilomanchi areas.

Two drilling targets are proposed in this study. The first is the intersection between the Chachimbiro and Azufral fault and the second is the Chachimbiro fault which is apparently most permeable area in the system. The choice of these targets is based on the structural, chemical and geophysical analysis done in this study. To reach these target two different locations are proposed for crossing the intersection of the faults and the third suggested a well should cross the Chachimbiro fault. From these locations, directional wells should be drilled to reach down to around 2000 m depth where the alleged reservoir is located.

A geological model derived using Petrel will be able to incorporate the new data from the well and the current conceptual model of the Chachimbiro area will be improved.

ACKNOWLEDGEMENTS

I would like to express my gratitude to Gunnlaugur M. Einarsson for his diligent assistance and advice during my research project, to Björn S. Hardarson for his support and constant monitoring of this project. I am genuinely grateful to Lúdvík S. Georgsson and Ingimar Gudni Haraldsson for the opportunity to take part in this amazing programme, to Málfrídur Ómarsdóttir, Thórhildur Ísberg and Markús A.G. Wilde for their commitment and unquestionable support during my stay and study in Iceland. I wish to give my thanks to ISOR and UNU-GTP staff, who sacrificed their time to share with us some of their knowledge and experiences.

My sincere gratitude to all my classmates for enjoying the time during this incredible experience, especially to Domi, Kristof, Zsófi, Danni, Fahman, Zoly, Bondi, James and Panni who helped me and made me feel special in different ways. Thanks a lot MA for those wonderful moments.

Sincere gratitude goes to Matilde Urquizo who thrusted and gave to me the opportunity to come to Iceland and also to Mario Brito for leading the development of our geothermal projects in Ecuador. Thanks to Danilo Asimbaya and Manabu Sugioka for their invaluable help during this project.

I would like to extend my gratitude to this paradise called Iceland, which is in my personal opinion one of the most extraordinary places in the world.

Finally, I want to dedicate this project to my family, to my mom Eva, my sister Michelle and my brother Richard. Everything I´ve done is for you.

REFERENCES

Abaya, J.G., D'Amore, F., and Arnórsson, S., 2000: Isotopes for geothermal investigations, *In:* Arnórsson, S (ed.), *Isotopic and chemical techniques in geothermal exploration, development and use, International Atomic Energy Agency, Vienna,* 49-65.

Aguilera, E., Cioni, R., Gherardi, F., Magro, G., Marini, L., and Pang Z., 2005: Chemical and isotope characteristics of the Chachimbiro geothermal fluids (Ecuador), *Geothermics, 34*, 495-517.

Almeida, E., Sandoval, G., Panichi, C., Noto, P., and Bellucci, L., 1990: Preliminary geothermal model of the volcanic areas in Ecuador, from chemical and isotopic studies of thermal manifestations. *Geothermal Investigations with Isotope and Geochemical Techniques in Latin America, Proceedings of the final research coordination meeting held in San José, Costa Rica,* 219-236.

Árnason, K., Karlsdóttir, R., Eysteinsson, H., Flóvenz, Ó.G., and Gudlaugsson, S.Th., 2000: The resistivity structure of high-temperature geothermal systems in Iceland. *Proceedings of the World Geothermal Congress 2000*, *Kyushu-Tohoku, Japan,* 923-928.

Arnórsson, S., Gunnlaugsson, E., and Svavarsson, H., 1983: The chemistry of geothermal waters in Iceland III. Chemical geothermometry in geothermal investigations. *Geochim. Cosmochim. Acta, 47*, 567-577.

Axelsson, G., 2013: Conceptual models of geothermal systems – Introduction. *Paper presented at Short Course V on Conceptual Modelling of Geothermal System, organized by UNUGTP and LaGeo, Santa Tecla, El Salvador*, UNU-GTP SC-16, 12 pp.

Beate, B., 1990: The volcanic complex Chachimbiro, first data and geothermal implications (in Spanish). *Proceedings of the 1st Conference in Earth Sciences, EPN, Quito,* November, 20-21.

Bernard, B., Robin, C., Beate, B., and Hidalgo, S., 2010: New evolutionary model and recent eruptive activity of the Chachimbiro volcano (in Spanish). *Proceedings of the SENAYCT conference*, 6 pp.

Bernard, B., Hidalgo, S., Robin, C., Beate, B., and Quijozaca, J., 2014: The 3640–3510 BC rhyodacite eruption of Chachimbiro compound volcano, Ecuador: a violent directed blast produced by a satellite dome. *Bull. Volcanol., 849,* 20 pp.

Cumming, W., 2009: Geothermal resource conceptual models using surface exploration data. *Proceedings of the 34th Workshop on Geothermal Reservoir Engineering, Stanford University, Stanford, CA*, 6 pp.

D'Amore, F., and Arnórsson, S., 2000: Geothermometry. In: Arnórsson, S. (ed.), *Isotopic and chemical techniques in geothermal exploration, development and use. Sampling methods, data handling, interpretation*. International Atomic Energy Agency, Vienna, 152-199.

Ego, F., Sébrier, M., Lavenu, A., Yépez, H., and Egüez, A., 1996: Quaternary state of stress in the Northern Andes and restraining bend model for the Ecuadorian Andes. *Tectonophysics, 259*, 101-116.

EOS, 2007: *Geophysics foundations: Physical properties: Electrical resistivity of geologic materials.* Department of Earth, Ocean and Atmospheric Sciences, website: *www.eos.ubc.ca/ubcgif/iag/foundations/properties/resistivity.htm*

Fournier, R.O., 1979: A revised equation for Na-K geothermometer. *Geoth. Res. Council, Trans., 3,* 221-224.

GeothermEx Inc., 2011: *Initial feasibility study to develop a conceptual model for Chachimbiro geothermal project* (in Spanish). Corporación Eléctrica del Ecuador - CELEC EP and Servicios y Remediación - SYR; technical report prepared by GeothermEx, Inc., 110 pp.

Giggenbach, W.F., 1986: Graphical techniques for the evaluated water/rock equilibration conditions by use of Na, K, Mg and Ca contents of discharge water. *Proceedings of the 8th New Zealand Geothermal Workshop, Auckland, NZ,* 37-43.

Giggenbach, W.F., 1988: Geothermal solute equilibria. Derivation of Na-K-Mg-Ca geoindicators. *Geochim. Cosmochim. Acta, 52*, 2749-2765.

Granda, B., 2011: *Geological mapping 1: 25000 of the pre-Quaternary rocks, Chachimbiro geothermal project, pre-feasibility phase* (in Spanish). Technical report prepared for SyR, 18 pp.

Hofstede, R., Calles, J., Lopez, V., Polanco, R., Torres, F., Ulloa, J., Vasquez, A. and Cerra, M., 2014: *The Andean moors - what do we know? State of knowledge about the impact of climate change on the moors ecosystem* (in Spanish). UICN, Quito, Ecuador, 154 pp.

Hall, M., 2012: *Geological mapping in 1:25,000 of the Chacana geothermal project area.* Technical report for SyR, January, 94 pp.

Lonsdale, P., 2005: Creation of the Cocos and Nazca plates by fission of the Farallon plate. *Tectonophysics, 404*, 237-264.

Lumb, J.T., 1981: Prospecting for geothermal resources. In: Rybach, L, and Muffler, P.L.J. (eds.) *Geothermal systems: principles and case histories*. Wiley-Interscience, Chichester, Sussex and NY, 77-108.

McCourt, W.J., Duque, P., and Pilatasig, L.F., 1997: *Geology of the Western Cordillera of Ecuador between 1–2°S: Quito, Ecuador*. Development Corporation and Geological Research, Mining and Metalurgy, British Geological Survey, project of the Mining and Environmental Control Department, Cartographic Information Program and geology report 3; scale 1:200,000.

MMC-MMTEC, 2016: *Preparatory study for the construction project geothermal plant in Chachimbiro. Progress report (Stage 2)* (in Spanish). Mitsubishi Materials Techno Corporation - Mitsubishi Materials Corporation, report for CELEC EP, August, 178 pp.

Nieva, D., and Nieva, R., 1987: Developments in geothermal energy in Mexico, part 12-A: Cationic composition geothermometer for prospection of geothermal resources. *Heat Recovery Systems and CHP, 7,* 243-258.

Palacky, G.J., 1987: Resistivity characteristics of Geologic targets. In: *Electromagnetic methods in applied geophysics, 1. Theory.* Soc. Expl. Geophys., Tusla, OK, USA.

Ponce, M., 2011: *Alteration map for the Chachimbiro geothermal project, Imbabura, Ecuador* (in Spanish). Technical report for SyR, September, 21 pp.

Powell, T., and Cumming, W., 2010: Spreadsheets for geothermal water and gas geochemistry, *Proceedings of the 35th Workshop on Geothermal Reservoir Engineering, Stanford University, Stanford, CA*, 393-402.

Ruiz, G., 2011: *Technical information, geological map, 1:25,000 of a part of the volcano, Chachimbiro geothermal project, prefeasibility phase* (in Spanish). Technical report for SyR, July, 1-55.

Ruiz, M., 2011: *Microseismic studies for the Chachimbiro geothermal project (in Spanish)*. Technical report for SyR, November, 1-38.

Sakindi, G., 2015: *Three-dimensional inversion of magnetotelluric data: geological/geothermal interpretation of Asal geothermal field, Djibouti*, University of Iceland, MSc thesis, UNU-GTP, Iceland, report 4, 90 pp.

Schellart, W.P., Freeman, J., Stegman, D.R., Moresi L. and May, D., 2007: Evolution and diversity of subduction zones controlled by slab width. *Nature, 446*, 308-311.

Schlumberger, 2016: *Petrel E&P software platform*. Schlumberger, website: *www.software.slb.com/products/petrel*

SYR, 2012: *Initial prefeasibility study to develop a conceptual model for the Chachimbiro geothermal project.* Servicios y Remediación – SYR, final report prepared for CELEC EP, Ecuador, 123 pp.

Spikings, R.A., Winkler, W., Seward., and Handler, R., 2001: Along-strike variation in the thermal and tectonic response of the continental Ecuadorian Andes to the collision with heterogeneous oceanic crust. *Earth and Planetary Science Letters, 186*, 57-73.

Steingrímsson, B., 2009: Geothermal exploration and development from a hot spring to utilization. *Paper presented at "Short Course on Surface Exploration for Geothermal Resources", organized by UNU-GTP and LaGeo, in Ahuachapan and Santa Tecla, El Salvador*, UNU-GTP SC-09, 8 pp.

Tikhonov, A. N., 1950: *The determination of electrical properties of the deep layers of the Earth's crust*. Dokl. Aad. Nauk. SSR 73: 295-297 (in Russian).

Tonani, F., 1980: Some remarks on the application of geochemical techniques in geothermal exploration. *Proceedings, Adv. Eur. Geoth. Res., 2nd Symposium, Strasbourg*, 428-443.

Vallejo, C., 2007: *Evolution of the western cordillera in the Andes of Ecuador (Late Cretaceous-Paleogene).* Swiss Federal Institute of Technology, Zürich PhD thesis, report ETH 17023, 208 pp.

Wrightson, B., 2011: *Analysis of structural geology data for Chachimbiro geothermal project.* Technical report for SYR, December, 6 pp.

Yang, C.S., Kao, S.P., Lee, F.B., and Hung, P.S., 2004: Twelve different interpolation methods: a case study of Surfer 8.0. *Proceedings of the XX ISPRS Congress, Istanbul,* 772–777.

Yock, A., 2009: Geothermometry. *Paper presented at "Short Course on Surface Exploration for Geothermal Resources", organized by UNU-GTP and LaGeo, in Ahuachapan and Santa Tecla, El Salvador*, UNU-GTP SC-09, 8 pp.

APPENDIX 1: Tables with geoscientific data

TABLE 1. Cross-section coordinates in Geographic Coordinate System: WGS 84 UTM zone 17S, used in order to create a resistivity data grid in Petrel

Cross-section		North	East
Cs-NE-SW-01	**East**	10055017.67	806411.23
	West	10048621.89	800015.45
Cs-NE-SW-02	**East**	10046728.61	802364.81
	West	10052774.37	805440.73
Cs-NE-SW-03	**East**	10046728.61	804486.13
	West	10053092.57	807455.98
Cs-NE-SW-04	**East**	10052790.28	808638.62
	West	10045599.53	806463.73
CS-E-W-05	**East**	10052456.17	801940.55
	West	10052456.17	808728.77
CS-E-W-06	**East**	10050653.05	800985.95
	West	10050653.05	808198.44
CS-E-W-07	**East**	10049698.46	802576.94
	West	10049698.46	808092.38
CS-E-W-08	**East**	10048531.73	802046.61
	West	10048531.73	808410.58
CS-E-W-09	**East**	10046940.74	807243.85
	West	10046940.74	802152.68
Cs-NW-SE-10	**East**	10053304.70	802152.68
	West	10047577.14	807880.25
Cs-NW-SE-11	**East**	10052578.15	800970.04
	West	10047683.20	805864.99

TABLE 2. Low-resistivity anomaly dimensions

Resistivity [Ωm]	Anomaly	Topography altitude above anomaly centre [m a.s.l.]	Altitude at which anomaly appears [m a.s.l.]	Thickness [m]	Estimated area [km^2]
1-3	1	3559	3400	374	0.41
	2	3039	2900	129	0.17
	3	3404	3200	177	0.81
	4	3106	2900	129	0.15
	5	3372	2900	203	0.38
	6	2707	1900	622	6.88
3-5	1	3570	3500	356	0.51
	2	3330	3250	200	3.28
	3	2697	2000	736	9.13
5-7	1	3441	3234	295	5.44
	2	2691	2452	289	0.43
	3	2721	2127	1078	10.77
	4	3956	3252	52	0.13
7-10	1	3455	3414	388	11.07
	2	2794	2256	961	13.36
	3	3945	3253	65	0.34
10-15	1	3162	3420	340	31.73
	2	3958	3259	89	0.55

TABLE 3. Sample coordinates in geographic coordinate system: WGS 84 UTM zone 17S and physical parameters collected during field campaigns in 2005, 2011 and 2016

ID	X	Y	Sampling date	Location	Classification	Spring water temp [°C]	pH	EC [mS/m]
CCB-1	806309	10050611	15.4.2016	Qda. Chachimbiro	Spring water	57.9	6.37	464
CCB-2	804734	10050412	16.4.2916	Qda. Chachimbiro	Fresh water	11.2	6.16	22.9
CCB-3	806016	10050461	16.4.2916	Qda. Chachimbiro	Spring water	73.5	7.2	697
CCB-4	802789	10050579	17.4.2016	Azufral	Fresh water	9.7	7.22	18.04
CCB-5	803102	10049533	17.4.2016	Azufral	Spring water	17.6	5.6	27
CCB-6	807336	10050783	18.4.2016	Chachimbiro complex	Spring water	59.4	7.86	691
CCB-7	807184	10050638	18.4.2016	Chachimbiro complex	Spring water	58	6.43	721
CCB-8	808845	10050584	18.4.2016	Chachimbiro complex	Spring water	36.5	6.07	297
CCB-9	804014	10047195	18.4.2016	Timbuyacu	Spring water	41.3	6.69	514
CCB-10	803032	10049768	19.4.2016	Qda. Azufral	Fumarole gas	10.1	-	-
CCB-11	804474	1050426	11.6.2016	Sulfur Mine	Gas	-	-	-
40	804019	10047202	21.5.2011	Timbuyacu cement tank spr	Spring water/Gas	41	6.43	4940
45	803108	10049496	22.5.2011	Qda de Azufre stream at pt b	Spring water	-		
46	810987	10047346	23.5.2011	Spr at Qda Pigunchuela	Spring water	22	6.36	1023
47	811937	10047686	23.5.2011	Qda Pigunchuela Rock Joint Spr	Spring water	30	6.04	3850
48	809642	10056070	23.5.2011	Qda Pilomachi	Spring water	24.8	33	6.16
49	806769	10051268	24.5.2011	Santa Susana 1 / Caja 1 ojo	Spring water	48.7	6.41	4020
50	807347	10050796	24.5.2011	Chachimbiro Caja 1 spr	Spring water	60.9	7.72	6760
52	803092	10049406	25.5.2011	Qda de Azufre spr below trail	Spring water	13.8	2.85	904
41	807178	10050656	21.5.2011	Chachimbiro Caja 7 spr	Spring water	56.6	6.45	6900
43	803108	10049496	22.5.2011	Qda de Azufre point a	Gas	-	-	-
56	803108	10049496	22.5.2011	Qda de Azufre point a	Gas	-	-	-
68	803108	10049496	22.5.2011	Qda de Azufre point a	Gas	-	-	-
42	803108	10049496	22.5.2011	Qda de Azufre point b	Gas	-	-	-
55	803108	10049496	22.5.2011	Qda de Azufre point b	Gas	-	-	-
69	803108	10049496	22.5.2011	Qda de Azufre point b	Gas	-	-	-
44	803108	10049496	22.5.2011	Qda de Azufre point c	Gas	-	-	-
57	803108	10049496	22.5.2011	Qda de Azufre point c	Gas	-	-	-
70	803108	10049496	22.5.2011	Qda de Azufre point c	Gas	-	-	-
51	803034	10049847	25.5.2011	Qda Pijumbi	Gas	-	-	-
58	803034	10049847	25.5.2011	Qda Pijumbi	Gas	-	-	-
71	803034	10049847	25.5.2011	Qda Pijumbi	Gas	-	-	-
53	807178	10050656	26.5.2011	Chachimbiro Caja 7	Gas	-	-	-
59	807178	10050656	26.5.2011	Chachimbiro Caja 7	Gas	-	-	-
67	807178	10050656	26.5.2011	Chachimbiro Caja 7	Gas	-	-	-
40	804019	10047202	21.5.2011	Timbuyacu cement tank spr	Gas	-	-	-
54	804019	10047202	21.5.2011	Timbuyacu cement tank spr	Gas	-	-	-
4	807317	10050820	25.7.2001	Chachimbiro	Spring water	24.8	7.31	
18	807914	10050857	15.6.1999	Chachimbiro	Spring water	21.5	8.12	
15	807627	10050848	14.6.1999	Chachimbiro	Spring water	23.7	7.74	
16	807021	10050588	15.6.1999	Chachimbiro	Spring water	58.6	6.34	
1	807021	10050588	24.7.2001	Chachimbiro	Spring water	58.3	6.21	
17	807176	10050661	15.6.1999	Chachimbiro	Spring water	54.9	7	
2	807176	10050661	24.7.2001	Chachimbiro	Spring water	53.4	6.37	
19	807258	10050743	15.6.1999	Chachimbiro	Spring water	46.9	6.19	
3	807258	10050743	25.7.2001	Chachimbiro	Spring water	47.2	6.23	
14	807463	10050788	11.6.1999	Chachimbiro	Spring water	59.1	6.25	
5	807463	10050788	25.7.2001	Chachimbiro	Spring water	54.4	6.7	
6	801939	10051843	25.7.2001	-	Spring water	16.7	-	
7	800977	10053365	25-Jul-01	-	Spring water	17.6	-	
8	802017	10054025	25-Jul-02	-	Spring water	6.7	-	
9	804054	10047301	26.7.2001	-	Spring water	10.9	7.76	
11	803584	10047256	27.7.2001	-	Spring water	14.1	8.18	
10	804098	10047122	26.7.2001	Timbuyacu	Spring water	42.2	6.46	
13	803382	10047905	27.7.2001	Timbuyacu	Spring water	29.9	6.17	
12	805228	10048297	27.7.2001	Timbuyacu	Spring water	17.2		

TABLE 4: Chemical analysis of Chachimbiro water samples, collected during the field work by MMC-MMTEC (2016)

Sample label	Li	Na	K	Ca	Mg	SiO2	B	Cl	F	SO4	HCO3	CO3	NH4
CCB-1	2.7	677	107	74	29	141	25	1060	0.3	48	418	0	4.6
CCB-2	0	0	0	86.5	0	0	0	0	0	0	0	0	0
CCB-3	4.4	1190	187	24	14	148	39	1600	0.5	82	511	0	6.4
CCB-4	0	0	0	9	0	0	0	0	0	0	0	0	0
CCB-5	0.013	16	3.1	54.9	8.6	100	0.76	0.25	0.16	14	149	0	0.18
CCB-6	4.3	1150	148	124	52	127	41	1640	0.41	31	670	0	4.5
CCB-7	4.3	1140	136	4.5	51	123	43	1690	0.38	28	652	0	7.2
CCB-8	1.7	450	36	115.9	24	99	17	664	0.24	18	372	0	4.3
CCB-9	2	650	65	152	142	64	26	833	0.16	9.1	1700	0	3.8

Sample label	As	Rb	Cs	Sr	Ba	Fe	Mn	δ18O	δ2H	sum cations	sum anions	Charge Balance
CCB-1	0.56	0	0	0	0	0	0	-8.6	-70	38.91	37.77	1%
CCB-2	0	0	0	0	0	0	0	-8.6	-70	4.32	0.00	**100%**
CCB-3	0.91	0	0	0	0	0	0	-7.4	-67	59.88	55.24	4%
CCB-4	0	0	0	0	0	0	0	-12	-86	0.45	0.00	**100%**
CCB-5	0	0	0	0	0	0	0	-12	-82	4.24	2.75	**21%**
CCB-6	1.2	0	0	0	0	0	0	-7.2	-70	65.14	57.91	**6%**
CCB-7	1.4	0	0	0	0	0	0	-7.5	-70	58.51	58.96	0%
CCB-8	0.31	0	0	0	0	0	0	-8.6	-74	28.74	25.22	**7%**
CCB-9	0.014	0	0	0	0	0	0	-8.9	-72	49.70	51.56	-2%

TABLE 5: Resulting temperature based upon liquid geothermometer using *Plotting Spreadsheet* developed by Powell and Cumming in 2010

ID	Amorphous Silica	Alpha Cristobalite	Beta Cristobalite	Chalcedony conductive	Quartz conductive	Quartz adiabatic	Na-K-Ca	Na-K-Ca Mg corr	Na/K Fournier 1979	Na/K Truesdell 1976	Na/K Giggenbach 1988	Na/K Tonani 1980	Na/K Nieva & Nieva 1987	Na/K Arnórsson et al. 1983	K/Mg Giggenbach 1986
CCB-1	35	107	58	133	158	150	222	71	260	243	272	285	246	247	115
CCB-3	38	110	61	136	161	152	247	129	259	242	271	284	245	246	145
CCB-7	28	99	50	124	149	143	246	21	233	207	247	245	219	214	114
CCB-9	-4	63	16	85	114	113	187	11	217	188	232	223	204	195	80

APPENDIX II: Geothermometer analysis of Chachimbiro water samples

Amorphous silica and crysobalite do not reach equilibrium in geothermal systems. These minerals are affected by the processes dilution and precipitation. These geothermometers are applicable in exploitation and production phases of the geothermal systems but not applicable to the Chachimbiro system. Also these geothermometers show very low temperature in the Chachimbiro hot spring, which indicated dilution and precipitation processes.
Quartz is the most stable and least soluble form of solid silica. This geothermometer indicates temperature from 100 to 180°C. However, the solubility is controlled by chalcedony and amorphous silica which control the silica solubility preferentially over quartz (Yock, 2009). The average temperature estimated with this quartz geothermometer is around 140°C and with the geothermometer chalcedony around 120°C. These values are closer to the second and third model proposed by SYR (2012).

The high concentration of Mg is not usual in geothermal fluids. The high concentration of Mg (> 1 ppm) in Chachimbiro fluids is explained by mixing process with cold water close to the surface. Yock (2009) mentions that the geothermometer K/Mg is useful in chloride waters with Mg concentrations <1.0 ppm and that this geothermometer is very sensitive to C_K^2/C_{Mg} ratios. Any slight addition of Mg through mixing of shallow water with the deep fluid gives cooler temperatures. Thus, this geothermometer would not applicable to Chachimbiro hot springs.

The Na/K/Ca geothermometers application would show wrong temperatures due to high partial pressure of CO_2 and ion exchange among Na-K-Ca with Mg which produces precipitation of Ca. This geothermometer is not applicable in water with high concentration of Mg either. Thus, this geothermometer is not applicable in Chachimbiro hot springs.

APPENDIX III: Resistivity and hydrographic maps from the Chachimbiro area

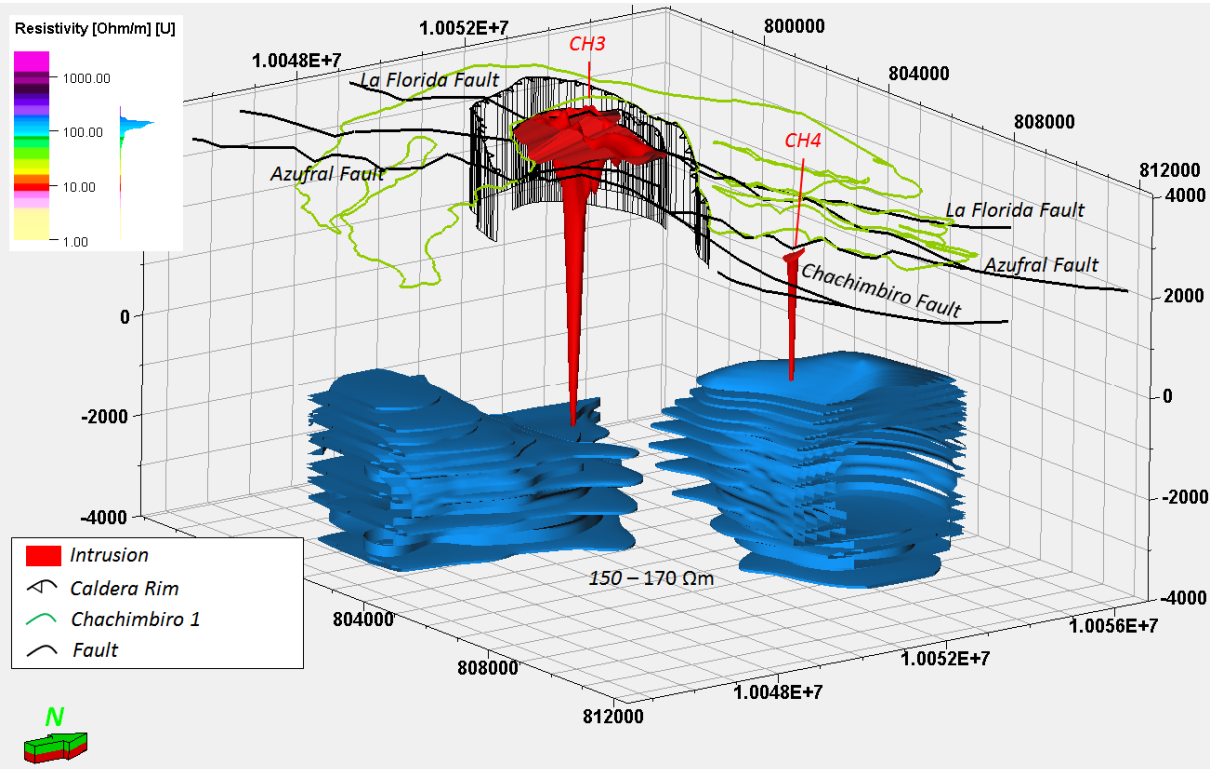

FIGURE 1: High-resistivity anomaly under Albují/Huga domes (CH3) main emission centre and under Chachimbiro emission centre (CH4)

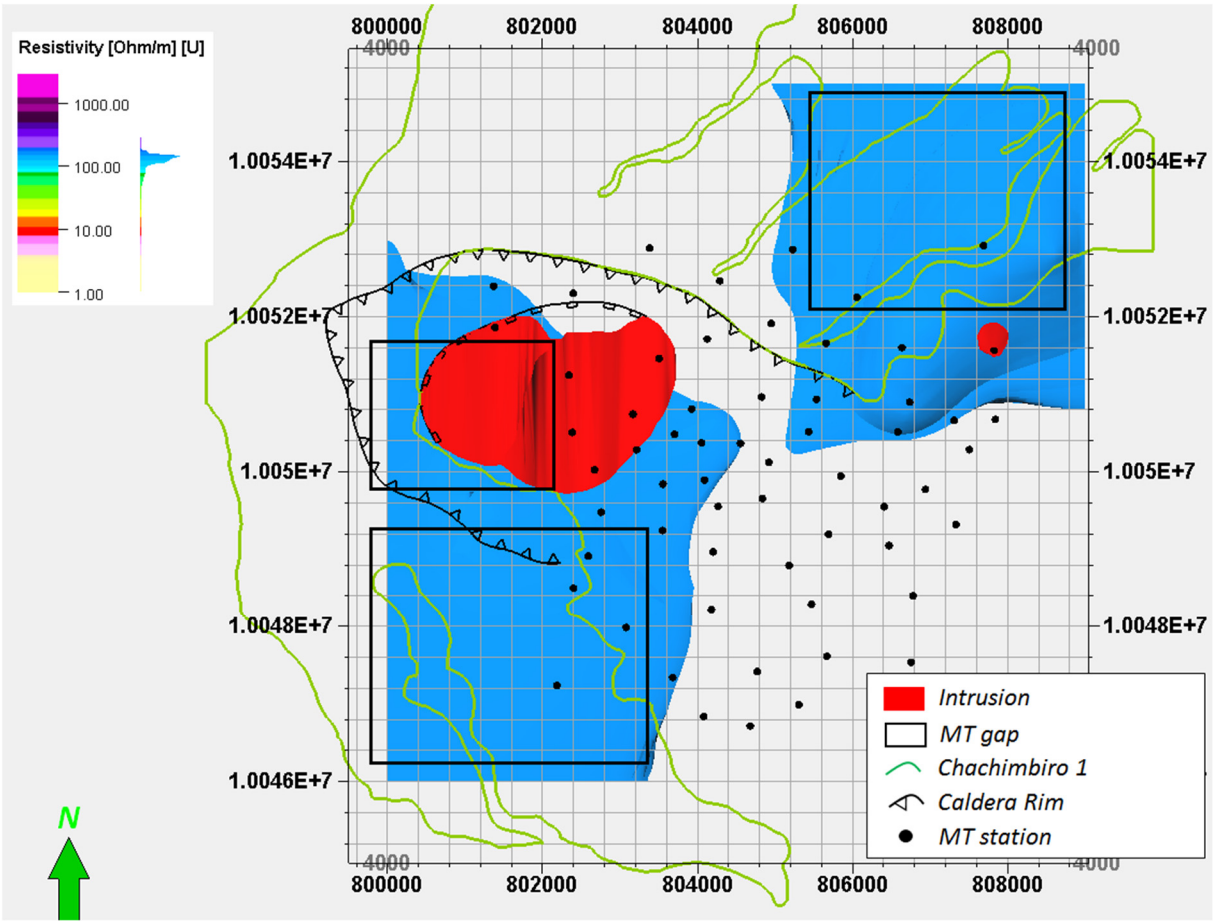

FIGURE 2: Magnetotelluric gaps that should be covered to confirm intrusions under the emission centres

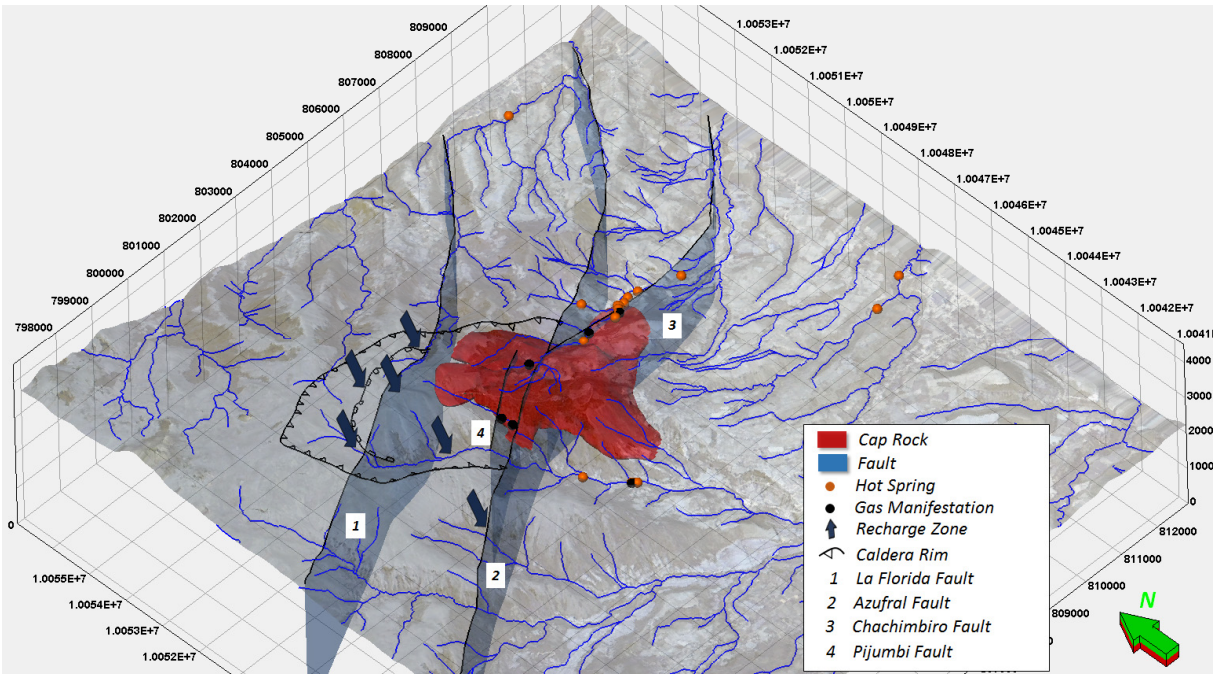

FIGURE 3: Hydrographic net at Chachimbiro volcanic complex and cold water recharge areas centres

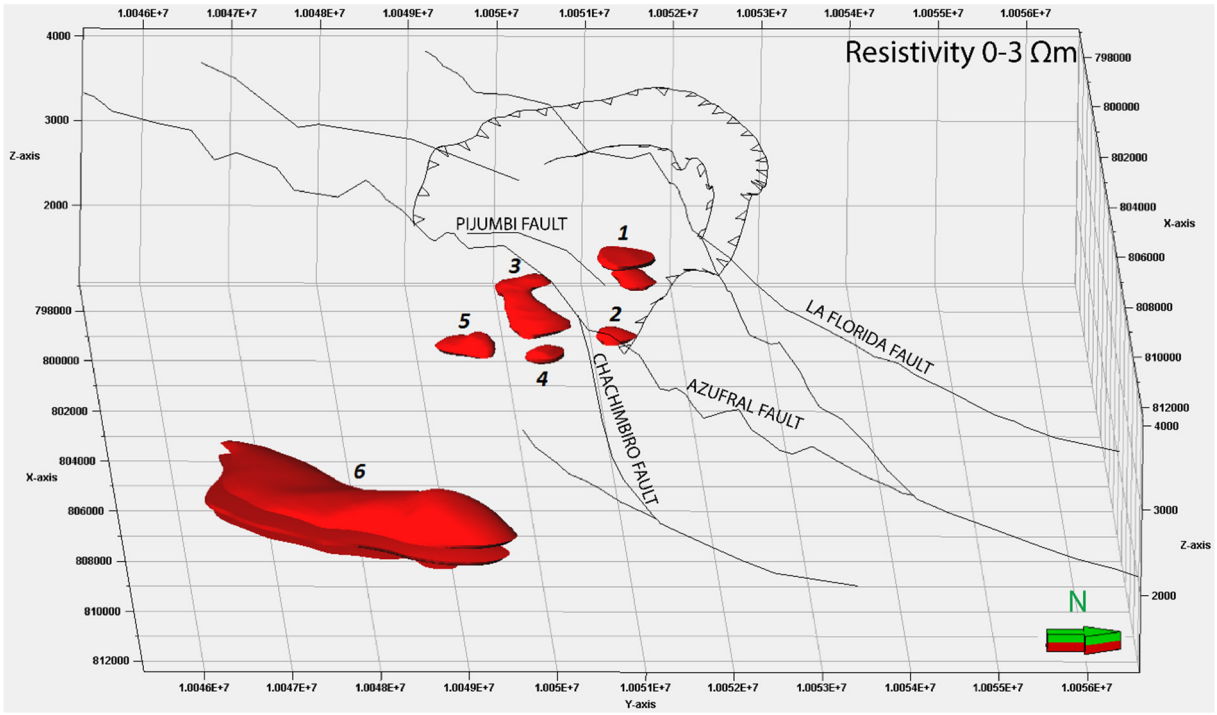

FIGURE 4: Low-resistivity anomalies for resistivity in the range 0-3 Ωm modelled in Petrel

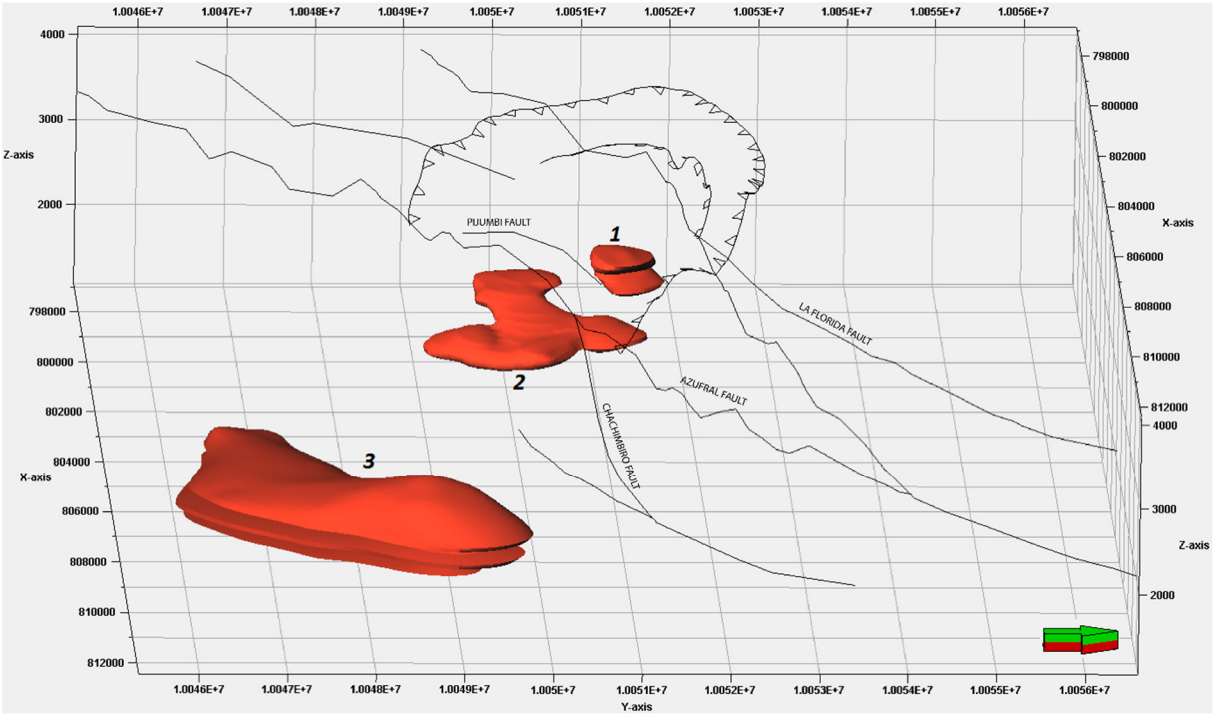

FIGURE 5: Low-resistivity anomalies for resistivity in the range 3-5 Ωm modelled in Petrel

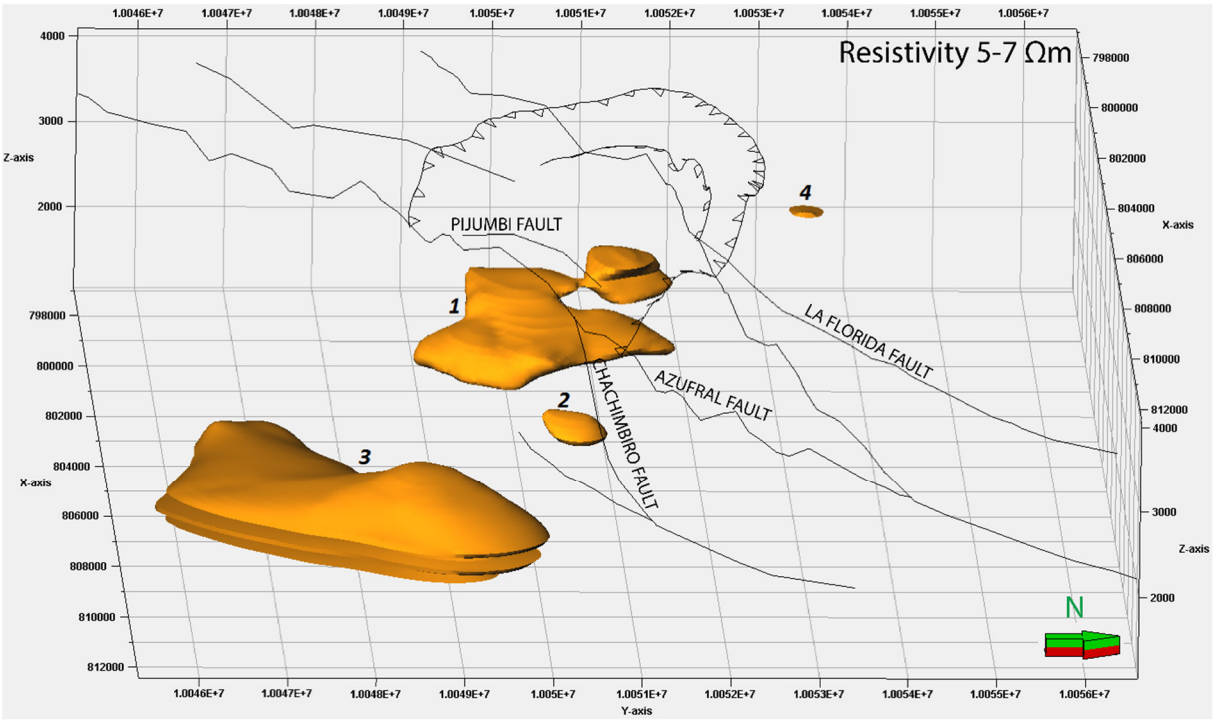

FIGURE 6: Low-resistivity anomalies for resistivity in the range 5-7 Ωm modelled in Petrel

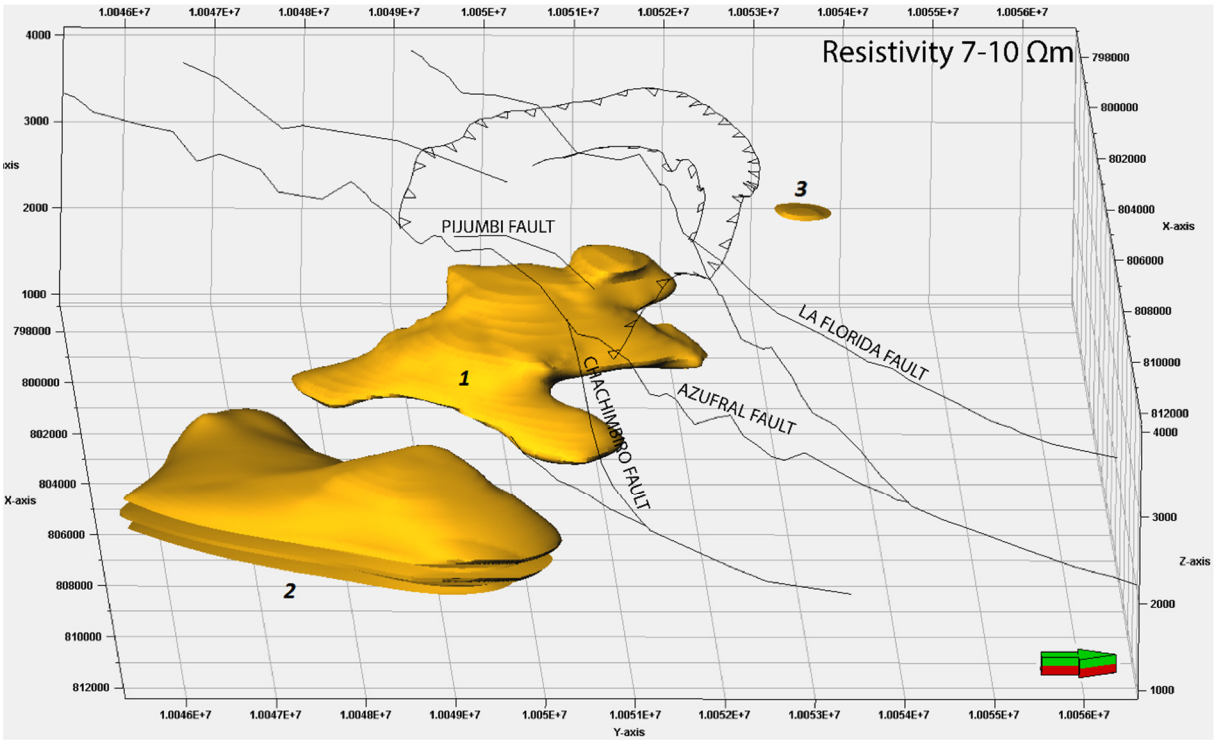

FIGURE 7: Low-resistivity anomalies for resistivity in the range 7-10 Ωm modelled in Petrel

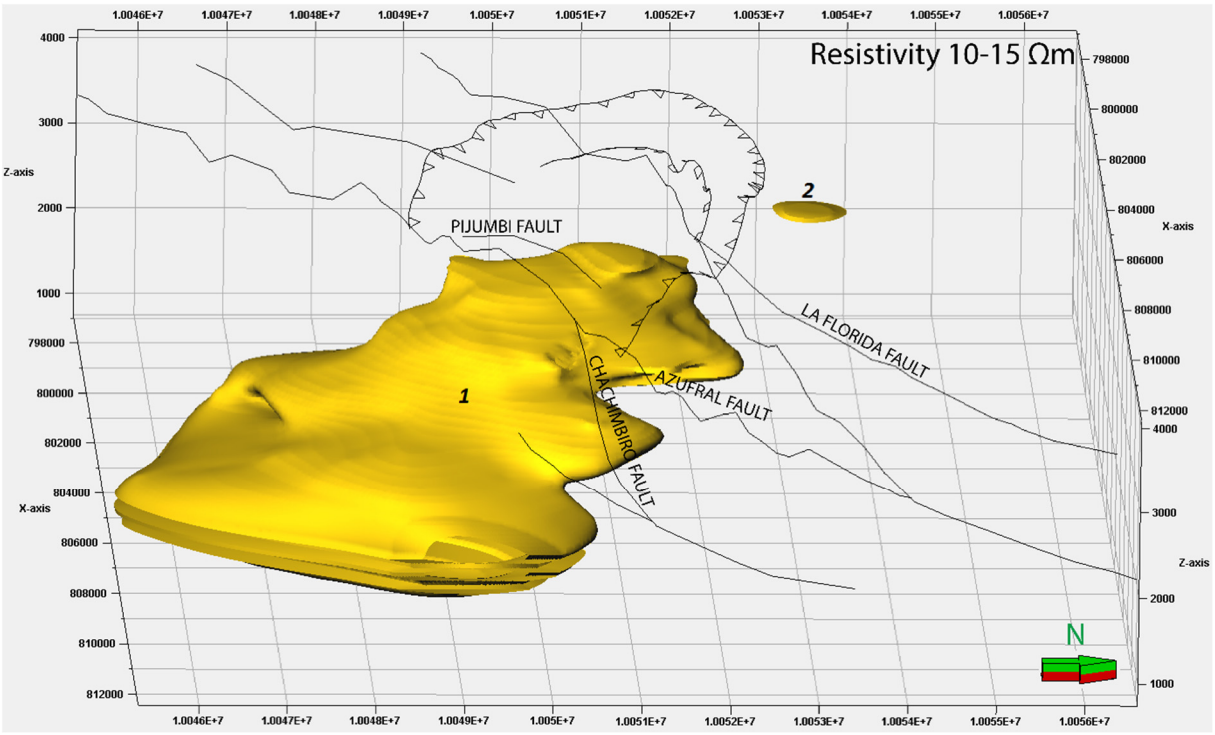

FIGURE 8: Low-resistivity anomalies for resistivity in the range 10-15 Ωm modelled in Petrel

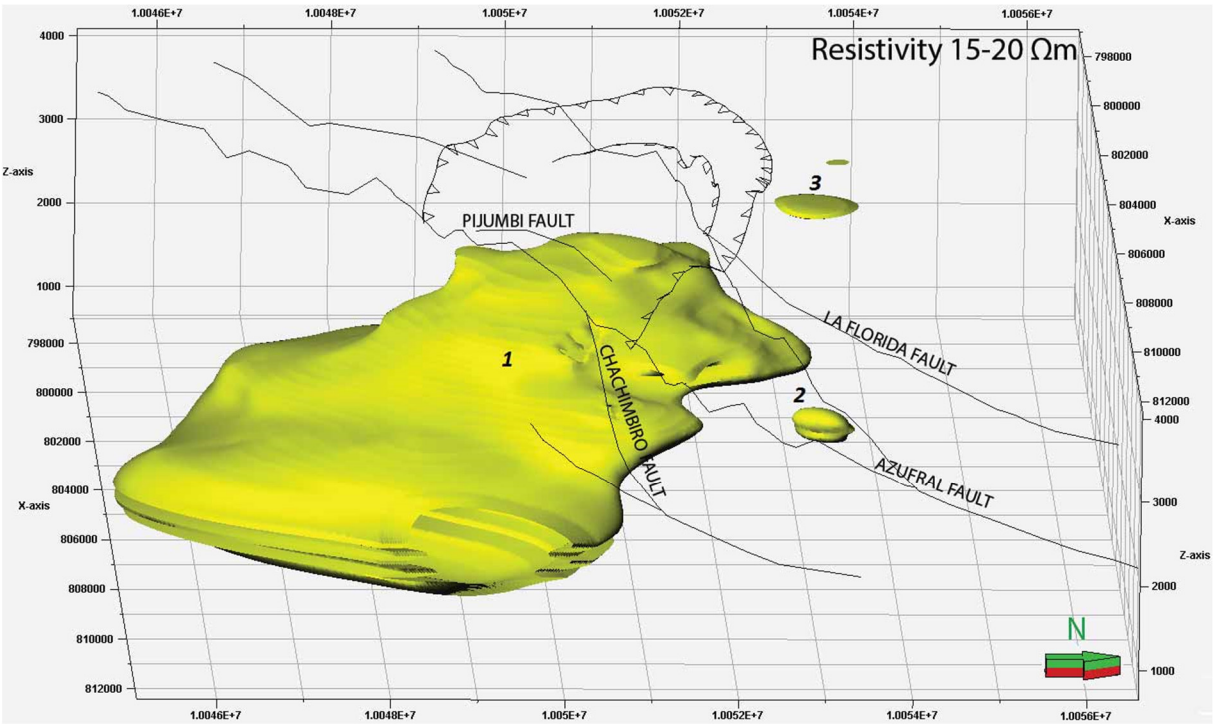

FIGURE 9: Low-resistivity anomalies for resistivity in the range 15-20 Ωm modelled in Petrel